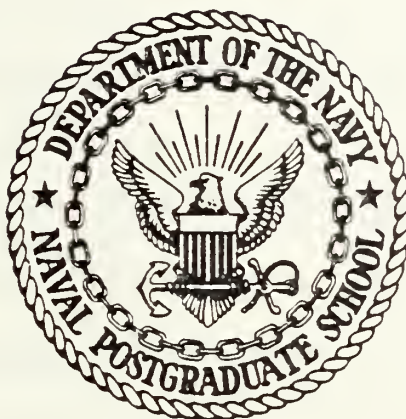


MEASUREMENT OF NEAR SEA SURFACE
TURBULENCE AND POSSIBLE WAVE INFLUENCE.

James H. Corbin

NAVAL POSTGRADUATE SCHOOL

Monterey, California



THESIS

MEASUREMENT OF NEAR SEA SURFACE
TURBULENCE AND POSSIBLE WAVE INFLUENCE

by

James H. Corbin

September 1977

Thesis Advisor:

K. L. Davidson

Approved for public release; distribution unlimited.

T180974
T180982

REPORT DOCUMENTATION PAGE		READ INSTRUCTIONS BEFORE COMPLETING FORM
1. REPORT NUMBER	2. GOVT ACCESSION NO.	3. RECIPIENT'S CATALOG NUMBER
4. TITLE (and Subtitle) Measurement of Near Sea Surface Turbulence and Possible Wave Influence		5. TYPE OF REPORT & PERIOD COVERED Master's Thesis; September 1977
		6. PERFORMING ORG. REPORT NUMBER
7. AUTHOR(s) James H. Corbin		8. CONTRACT OR GRANT NUMBER(s)
9. PERFORMING ORGANIZATION NAME AND ADDRESS Naval Postgraduate School Monterey, California 93940		10. PROGRAM ELEMENT, PROJECT, TASK AREA & WORK UNIT NUMBERS
11. CONTROLLING OFFICE NAME AND ADDRESS Naval Postgraduate School Monterey, California 93940		12. REPORT DATE September 1977
		13. NUMBER OF PAGES 72
14. MONITORING AGENCY NAME & ADDRESS (if different from Controlling Office) Naval Postgraduate School Monterey, California 93940		15. SECURITY CLASS. (of this report) Unclassified
		15a. DECLASSIFICATION/DOWNGRADING SCHEDULE
16. DISTRIBUTION STATEMENT (of this Report) Approved for public release; distribution unlimited.		
17. DISTRIBUTION STATEMENT (of the abstract entered in Block 20, if different from Report)		
18. SUPPLEMENTARY NOTES		
19. KEY WORDS (Continue on reverse side if necessary and identify by block number)		
20. ABSTRACT (Continue on reverse side if necessary and identify by block number) Measurements were made at three levels above the sea surface to observe possible wave influence on turbulence parameters. Two levels, at one and three meters above the sea surface, were mounted on a small floating platform tethered to the bow of the R/V Acania. The third level, at 6.6 meters above the sea surface, was mounted on a boom on the bow of the ship. Measurements were made of mean wind, mean temperature,		

mean humidity, and of the fluctuating temperatures and velocities at all three levels. These data were interpreted on the basis of empirically derived expressions describing the temperature structure function parameter, C_T^2 , and the rate of dissipation of turbulent kinetic energy, ϵ . For optical relevance, C_T^2 was related to C_N^2 , the refractive index structure function parameter.

Results show qualitatively that there is a substantial wave influence near the sea surface, and that the system and procedures used to obtain the data produce valid measurements for deriving the wave influence on turbulence and on optical transmission in the near sea surface layer adjacent to the waves.

Approved for public release; distribution unlimited.

MEASUREMENT OF NEAR SEA SURFACE
TURBULENCE AND POSSIBLE WAVE INFLUENCE

by

James H. Corbin
Lieutenant, United States Navy
B.S., University of Nebraska, 1971

Submitted in partial fulfillment of the
requirements for the degree of

MASTER OF SCIENCE IN METEOROLOGY AND OCEANOGRAPHY

from the
NAVAL POSTGRADUATE SCHOOL
September 1977

ABSTRACT

Measurements were made at three levels above the sea surface to observe possible wave influence on turbulence parameters. Two levels, at one and three meters above the sea surface, were mounted on a small floating platform tethered to the bow of the R/V Acania. The third level, at 6.6 meters above the sea surface, was mounted on a boom on the bow of the ship. Measurements were made of mean wind, mean temperature, mean humidity, and of the fluctuating temperatures and velocities at all three levels. These data were interpreted on the basis of empirically derived expressions describing the temperature structure function parameter, C_T^2 , and the rate of dissipation of turbulent kinetic energy, ϵ . For optical relevance, C_T^2 was related to C_N^2 , the refractive index structure function parameter.

Results show qualitatively that there is a substantial wave influence near the sea surface, and that the system and procedures used to obtain the data produce valid measurements for deriving the wave influence on turbulence and on optical transmission in the near sea surface layer adjacent to the waves.

TABLE OF CONTENTS

I.	INTRODUCTION - - - - -	11
II.	BACKGROUND - - - - -	13
	A. GENERAL THEORY - - - - -	13
	B. PLATFORM DESIGN - - - - -	24
III.	DATA COLLECTION - - - - -	27
	A. PLATFORM AND LOCATION - - - - -	27
	B. FLOATING PLATFORM DESIGN - - - - -	27
	C. INSTRUMENTATION AND PROCESSING EQUIPMENT - - - - -	30
IV.	ANALYSES PROCEDURES - - - - -	42
	A. ANALYSES OF MEAN DATA - - - - -	42
	B. ANALYSES OF PAIRED TEMPERATURE SENSORS - - - - -	43
	C. ANALYSES OF VELOCITY FLUCTUATION DATA - - - - -	45
	D. TEMPERATURE SENSOR AND HOT WIRE CALIBRATION - - - - -	50
V.	RESULTS - - - - -	52
VI.	CONCLUSIONS - - - - -	64
	APPENDIX A: DATA TABLES - - - - -	65
	LIST OF REFERENCES - - - - -	70
	INITIAL DISTRIBUTION LIST - - - - -	72

LIST OF FIGURES

1.	The dimensionless temperature structure function parameter versus the Richardson number - - - - -	22
2.	Joint probability-conditional mean results of σ_T/T_* for C/U_* and Z/L dependence - - - - -	23
3.	Dependence of the dimensionless mean-square temperature fluctuations σ_T/T_* on C/U_* - - - - -	24
4.	The dimensionless dissipation rate versus Richardson number - - - - -	25
5.	Optical ranges and R/V Acania position in Monterey Bay - - - - -	28
6.	Photograph of floating platform deployed from the bow of the R/V Acania - - - - -	31
7.	Photograph of sensor arrangement on floating platform - - - - -	32
8.	Sensor and instrumentation location on the R/V Acania - - - - -	33
9.	Three cup anemometer - - - - -	34
10.	Sensor arrangement at one level - - - - -	36
11.	Quartz thermometer probe - - - - -	38
12.	Aspirator - - - - -	39
13.	Lithium chloride humidity sensor - - - - -	40
14.	Example of strip chart section - - - - -	44
15.	Calibration plot for spectrum analyzer - - - - -	47
16.	Example of temperature variance spectra - - - - -	48
17.	Example of velocity variance spectra - - - - -	49
18.	Example plots of mean wind versus height - - - - -	53
19.	Normalized C_N^2 (computed from C_T^2) results versus height - - - - -	55

20.	Summary of results of low level DTSFP versus Richardson number - - - - -	57
21.	C_N^2 versus time - shipboard results compared to shore results for 2/15/77 - - - - -	58
22.	C_N^2 versus time - shipboard results compared to shore results for 2/16/77 - - - - -	59
23.	C_N^2 versus time - shipboard results compared to shore results for 2/17/77 - - - - -	60
24.	Normalized dissipation rate ϵ versus height - - - - -	61
25.	Plots of U_* versus height for each level and table of comparison of the means - - - - -	63

LIST OF SYMBOLS

C_N^2	Refractive index structure function parameter
C_T^2	Temperature index structure function parameter
DSFP	Dimensionless structure function parameter
DTSFP	Dimensionless temperature structure function parameter
ϵ	Rate of dissipation of turbulent kinetic energy
ϵ_θ	Rate of dissipation of temperature variance
f	Temporal frequency
g	Acceleration due to gravity
k	Wave number
L	Monin-Obukhov stability length
L_o	Outer scale, lower limit of inertial subrange
λ_o	Inner scale, upper limit of inertial subrange
P	Atmospheric pressure
n	Refractive index
r	Separation distance
Ri	Richardson number
$S(f \text{ or } k)$	Spectral density
T'	Temperature fluctuations
T_*	Scaling temperature
θ	Potential temperature
θ_v	Virtual potential temperature
\bar{U}	Mean horizontal wind speed
U_*	Scaling (friction) velocity

w	Vertical wind speed
χ	Temperature variance
Z	Height
Z/L	Stability parameter

ACKNOWLEDGEMENTS

I take this opportunity to express my heartfelt gratitude to Professor Ken Davidson, without whose patient and understanding advice, this project could never have been started let alone finished. Also, my sincerest thanks to Professor Tom Houlihan, Dr. Chris Fairall, and Professor Gordon Schacher, for their invaluable assistance in all areas. And to Ray Garcia and Charles Leonard, I will be eternally grateful for their on the spot assistance in helping me with the design and construction of the entire system.

And last, but not least by any means, I truly am thankful to my wife and children and to the good Lord, for giving me the inspiration and the tenacity to complete this thesis.

I. INTRODUCTION

Describing near sea surface variations of turbulence parameters is important in many areas such as the coupling between the wind and the waves or the overall heat budget of the atmosphere and the oceans. In this study the primary concern is limited to the effect of the near sea surface variations of the turbulence parameters on photographic resolution. In particular, the effects are most predominant when the line of sight is along or near the sea surface, as when viewing from a small craft, or when the line of sight is over the horizon.

Turbulence parameters investigated in this study were C_T^2 , the temperature structure function parameter, and ϵ , the rate of dissipation of turbulent kinetic energy. For optical wavelengths, C_N^2 , the index of refraction structure function parameter, has been shown to be directly related to C_T^2 . Both C_N^2 and ϵ are related to image resolution since C_N^2 describes the intensity of refractive index fluctuations and ϵ determines the micro-scale of turbulence.

Previous studies by Davidson, et al. (1977) of over water turbulence parameters have established the height variations of C_T^2 and ϵ for levels at least six meters above the water. However, there exist few data to verify the height variations of C_T^2 and ϵ within the first few meters above the water. It is the layer below six meters, adjacent to

the sea surface, that is of primary interest in this study. It is in this layer that the wave influence on turbulence parameters is expected to predominate.

Earlier studies have shown that C_T^2 and ϵ vary inversely with height depending on the stability of the atmosphere in that layer. The inverse relationship suggests that the higher turbulence can be expected nearest the sea surface. In the earlier studies, the wave influence was not examined thoroughly. It is suspected that the wave influence on the turbulence adjacent to the sea surface would increase the turbulence over waves compared to the turbulence over a flat sea surface.

The nature and scope of this study is primarily to establish procedures for making measurements of the turbulence parameters C_T^2 and ϵ in the layer adjacent to the sea surface and in the presence of some wave action, mainly swell. Measurements were made from about six meters above mean sea level to within one meter of the actual sea surface. The levels are defined in reference to the surface of the longer period swell waves. Secondly, the results of these measurements were analyzed to see if any wave influence could be inferred, and if so, if there was any correlation to the variations in the photographic resolution when the line of sight was through the layer adjacent to the sea surface.

II. BACKGROUND

A. GENERAL THEORY

As stated, the primary concern of this study is the effect of the variations of turbulence parameters on the photographic resolution when the transmission path is near the sea surface. Image resolution has been empirically related to the scale of the refractive index inhomogeneities and to the intensity of fluctuations in the refractive index. These in turn can be related to the refractive index structure function, C_N^2 , which can be directly related to the temperature structure function parameter, C_T^2 , and to the rate of dissipation of turbulent kinetic energy, ϵ . Similarity expressions exist which relate C_T^2 and ϵ to mean conditions. The observation objectives of this study were to measure and analyze the mean temperature, wind speed, and humidity immediately adjacent to the sea surface.

In turbulence theory, it is important to consider whether the turbulence is isotropic or anisotropic. In general, large scale turbulence is anisotropic and small scale turbulence is isotropic. The universal formulae considered are valid only for isotropic small scale turbulence.

Kolmogorov (1941) postulated that small scale turbulence should be isotropic even though it was generated by and embedded in anisotropic large scale turbulence. If the Reynolds numbers are large enough, the turbulence will adjust

through inertial transfer and viscous dissipation until a statistical equilibrium is reached.

Since the small scale fluctuations are isotropic in nature, only one parameter is necessary to describe the intensity of the refractive index fluctuations over many scales. It is the refractive index structure function parameter, C_N^2 , defined as

$$C_N^2 = [\langle n(x) - n(x+r) \rangle]^2 / r^{2/3} \quad (1)$$

where $n(x)$ and $n(x+r)$ are refractive indices at two points on a line oriented normal to the mean wind direction and separated by the distance r , which is less than the outer scale, L_0 , the lower end of the inertial subrange, and greater than the inner scale, ℓ_0 , the smallest scale of naturally occurring turbulence.

The refractive index is determined primarily by density fluctuations and can therefore be related to temperature fluctuations. Neglecting humidity effects with respect to optical wavelengths, the expression relating C_N^2 to C_T^2 is

$$C_N^2 = [79. \times 10^{-6} P/T^2]^2 C_T^2 \quad (2)$$

The expression defining the temperature structure function parameter is similar to the one for C_N^2 and is

$$C_T^2 = [\langle T'(x) - T'(x+r) \rangle]^2 / r^{2/3} \quad (3)$$

where $T'(x)$ and $T'(x+r)$ are temperature fluctuations at two points separated by the distance r .

Practical meteorological and optical methods for direct measurement of C_N^2 and C_T^2 have been developed.

An alternate relationship for C_T^2 , based on measurements of the dissipation of turbulent kinetic energy, ϵ , and temperature variance, χ , is

$$C_T^2 = \beta \chi \epsilon^{-1/3} \quad (4)$$

where β is an empirical constant with a value of 3.2. This form enables indirect estimates of C_T^2 to be made from the mean conditions, since ϵ and χ are easily related to boundary layer fluxes and to profiles when steady horizontally homogeneous conditions exist.

Small scale velocity fluctuation properties are also of interest in optical propagation because image resolution has been empirically related to the inner scale, ℓ_0 , which is defined as

$$\ell_0 = (\gamma^3 / \epsilon)^{1/4} \quad (5)$$

where γ is the kinematic molecular viscosity. ϵ can be obtained from either one-dimensional velocity variance spectral estimates in the inertial subrange or from velocity structure function estimates.

Based on empirically derived expressions, ϵ and χ can be functionally related to mean profile and flux estimates (U_* , T_* , Z/L) resulting in the following relationships

$$\epsilon = \frac{U_*^3}{kZ} \phi_1(Z/L) \quad (6)$$

and

$$\chi = \frac{U_* T_*^2}{kZ} \phi_2(Z/L) \quad (7)$$

L is the "Monin-Obukhov" stability length and is defined as

$$L = \frac{-\bar{\theta} U_*^3}{gk \bar{\theta}_v' w} \quad (8)$$

Businger, et al. (1971), empirically determined the forms of $\phi_1(Z/L)$ and $\phi_2(Z/L)$ as

$$\phi_1\left(\frac{Z}{L}\right) = \begin{cases} (1 - 15 Z/L)^{1/4} - Z/L, & \frac{Z}{L} \leq 0 \\ 1 + 3.7 Z/L, & \frac{Z}{L} \geq 0 \end{cases} \quad (9)$$

$$\phi_2\left(\frac{Z}{L}\right) = \begin{cases} 0.74(1 - 9 Z/L)^{-1/2}, & \frac{Z}{L} \leq 0 \\ 0.74 + 4.7 Z/L, & \frac{Z}{L} \geq 0 \end{cases} \quad (10)$$

where $-Z/L$ and $+Z/L$ correspond to unstable and stable conditions.

It is desirable to have expressions which relate C_T^2 and λ_0 at some level, Z , to parameters which can be estimated from more readily available mean parameters. Such parameters are boundary fluxes (U_* and T_*) or mean gradients obtained from multiple level measurements or the wind at a given level and an air-water temperature difference. Such relationships are

$$C_T^2 = T_*^2 Z^{-2/3} \phi_3(Z/L) \quad (11)$$

where

$$\phi_3\left(\frac{Z}{L}\right) = k^{-2/3} \phi_1\left(\frac{Z}{L}\right)^{-1/3} \phi_2\left(\frac{Z}{L}\right)$$

A formulation for $\phi_3(Z/L)$ was obtained by Wyngaard, et al. (1971) on the basis of overland data. Their formulation was

$$\phi_3(Z/L) = 4.9[1-7(Z/L)]^{-2/3}, \quad 0 \leq Z/L \quad (12)$$

$$\phi_3(Z/L) = 4.9[1+2.75(Z/L)]^{-2/3}, \quad 0 \leq Z/L \quad (13)$$

An examination of Equations (11), (12), and (13) with the knowledge that T_*^2 is independent of height in the surface layer yields the following general predictions for the height variations of C_T^2 :

- i) For near neutral conditions, ($Z/L = 0$), C_T^2 will decrease with height as $Z^{-2/3}$, since Equation (11) becomes

$$C_T^2 = T_*^2 Z^{-2/3}, \quad (14)$$

where T_*^2 is independent of height.

- ii) For unstable conditions ($Z/L \leq 0$), C_T^2 will decrease more rapidly with height than $Z^{-2/3}$. If $-7 Z/L \gg 1$, C_T^2 should decrease with height as approximately $Z^{-4/3}$ since Equation (11) can be expressed as

$$C_T^2 \approx \frac{4}{3} \left(\frac{T}{kg}\right)^{2/3} (\overline{wT'})^{4/3} Z^{-4/3} \quad (15)$$

where $\left(\frac{T}{kg}\right)^{2/3} (\overline{wT'})^{4/3}$ is independent of height.

- iii) For stable conditions ($Z/L \geq 0$), C_T^2 will decrease with height less rapidly than $Z^{-2/3}$. A limiting expression, such as Equation (13) for $-7 Z/L \gg 1$, is not considered for this case since at large positive values of Z/L , mechanical turbulence is nonexistent.

The inner scale, ℓ_o , can also be related to the boundary fluxes and mean gradients in the expression

$$\ell_o = [kZ\gamma^3/U_*^3 \phi_1(\frac{Z}{L})]^{1/4} \quad (16)$$

An examination of ϵ on the basis of Equations (6) and (9), with the knowledge that U_*^3 and L are independent of height in the surface layer, yields the following general expressions for the variation of ϵ with height.

- i) For neutral conditions ($Z/L = 0$), ϵ will decrease with height as Z^{-1} since Equation (6) becomes

$$\epsilon = \frac{U_*^3}{k} Z^{-1} \quad (17)$$

- ii) For stable conditions ($Z/L > 0$), ϵ will decrease less rapidly with height than Z^{-1} since Equation (6) becomes

$$\epsilon = \frac{U_*^3}{k} Z^{-1} (1 + 3.7 Z/L) \quad (18)$$

and $(1 + 3.7 Z/L)$ increases with height.

- iii) For unstable conditions ($Z/L < 0$), ϵ will also decrease less rapidly with height than Z^{-1} , since Equation (6) becomes

$$\epsilon = \frac{U_*^3}{k} Z^{-1} [(1 - 15 \frac{Z}{L})^{-\frac{1}{4}} - \frac{Z}{L}] \quad (19)$$

and the quantity in brackets, $\phi_1(Z/L)$, increases with increasing height. However, this increase with height is less than for the stable case, so the decrease of ϵ with height in the unstable case is less than for the stable case.

Selecting the mean wind at two appropriate levels (Z_1 and Z_2) and when conditions are at or near neutral, U_* can be estimated from the mean wind observation as

$$U_* = k(\bar{U}_2 - \bar{U}_1)/\ln(Z_2 - Z_1) \quad (20)$$

Furthermore, when conditions are at or near neutral, the production of turbulent kinetic energy is considered to be equal to the dissipation of turbulent kinetic energy, yielding

$$U_* = (\epsilon k Z)^{1/3} \quad (21)$$

The relationships given by Equations (20) and (21) allow U_* estimates from either mean wind profiles or from velocity fluctuation data.

Alternate expressions for C_T^2 and ϵ based on profile gradients and the Richardson number (Ri) as the stability parameter are

$$C_T^2 = Z^{4/3} (\partial \bar{\theta} / \partial Z)^2 \phi_4(Ri) \quad (22)$$

$$\text{and} \quad \epsilon = (kZ)^2 (\partial \bar{U} / \partial Z)^3 \phi_5(Ri) \quad (23)$$

$$\text{with} \quad Ri = \frac{(g/T) (\partial \bar{\theta}_v / \partial Z)}{(\partial \bar{U} / \partial Z)} \quad (24)$$

where $\phi_4(Ri)$ and $\phi_5(Ri)$ are empirically derived and formulated on the basis of observations of temperature and

velocity, fluctuations and mean gradients of wind speed, temperature, and humidity, and where $\bar{\theta}_v$ is the mean virtual potential temperature, $\bar{\theta}_v = \bar{\theta}(1 + 0.61 q)$. A formulation of $\phi_4(Ri)$ was given by Wyngaard et al. (1971).

A comparison of 368 overwater C_T^2 and profile results with the overland empirical expression, Equation (22), appears in Figure 1. The distribution predicted by Equation (22) is the solid line. The circles are mean dimensionless temperature structure function parameter (DTSFP) results over .50 Richardson number (Ri) intervals. The standard deviation corresponding to each mean value appears as a vertical line on which the number of values defining the mean appears. Larger DTSFP values for the overwater regime for near neutral and stable conditions ($Ri > -.5$) can be qualitatively related to the wave influence. Decreased DTSFP values for unstable conditions ($Ri < -.5$) are, perhaps, associated with aerodynamic smooth properties for the sea surface during light wind conditions.

Evidence of wave influence on C_T^2 appears in joint probability-conditional mean results of the normalized temperature variance (σ_T^2/T_*^2) over waves in Figure 2. The results and the measurements yielding them are described in Davidson (1974). The ratio $(\sigma_T/T_*)^2$ is directly related to the DTSP, Wyngaard, et al. (1971). In Figure 2 the vertical axis variable (C/U_*) defines wave influence on σ_T/T_* , C is the phase speed of prevailing swell, L is the Monin-Obukhov stability length. The results were obtained under near stable conditions. The increase of the conditional mean of σ_T/T_* ,

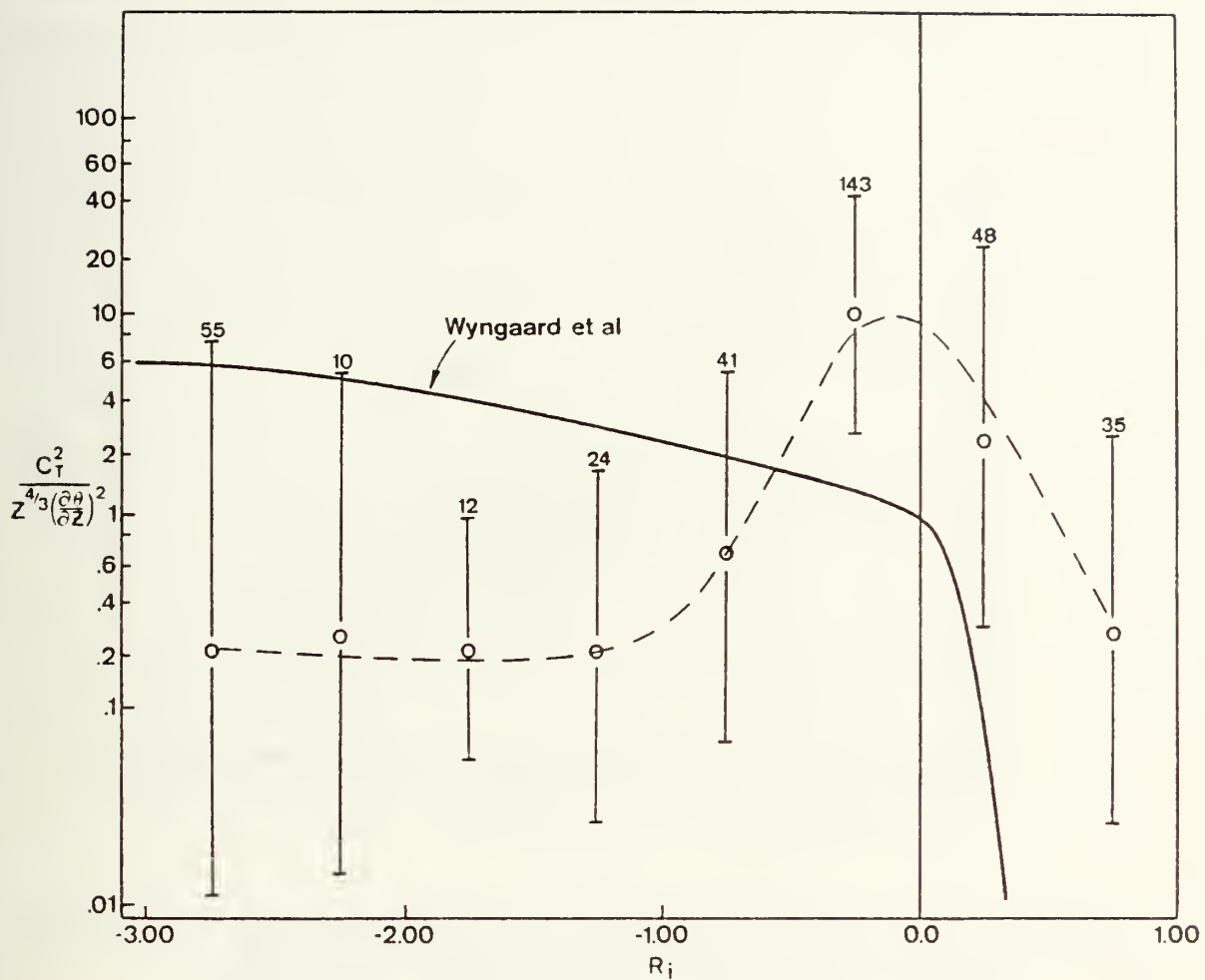


Figure 1. The dimensionless temperature structure function parameter versus the Richardson number.

values appear as numbers on the grid, for increasing C/U_* for near neutral conditions, ($Z/L < .1$), provides qualitative evidence that the wave influence (C/U_*) on σ_T/T_* , hence the DTSP, could be as significant as the stability influence (Z/L).

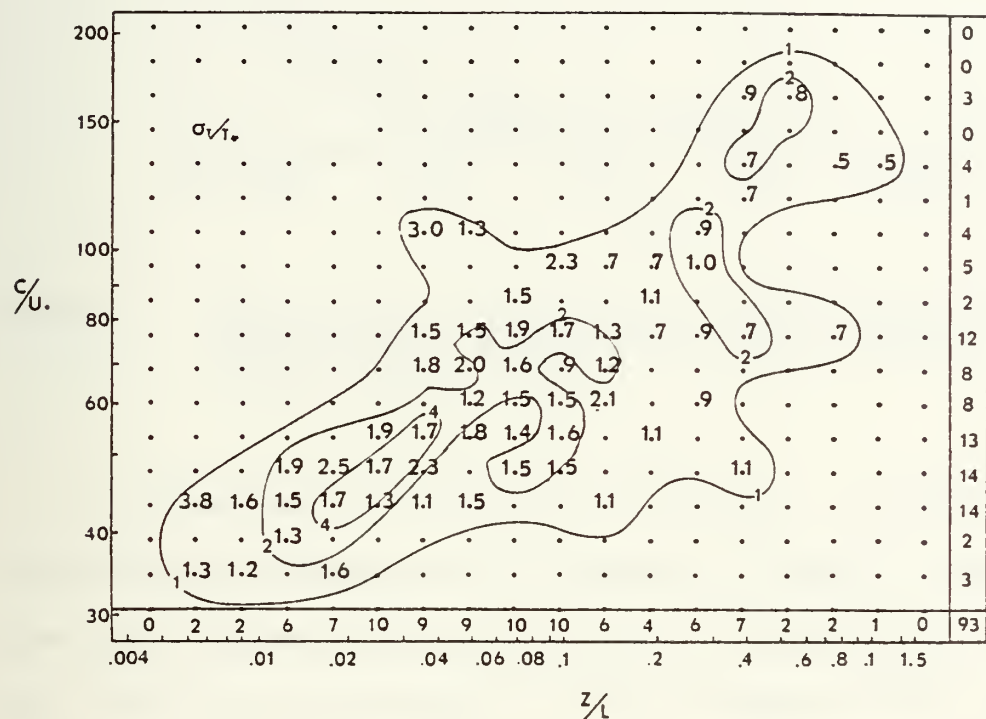


Figure 2. Joint probability-conditional mean results of σ_T/T_* for C/U_* and Z/L dependence. (From Davidson, 1974)

Volkov (1969) also described a wave influence on σ_T/T_* . His results, Figure 3, were from measurements during unstable conditions and established a decrease in σ_T/T_* due to the wave influence, C/U_* . This results agrees with those shown in Figure 1, where under unstable conditions the DTSP is less than the overland prediction.

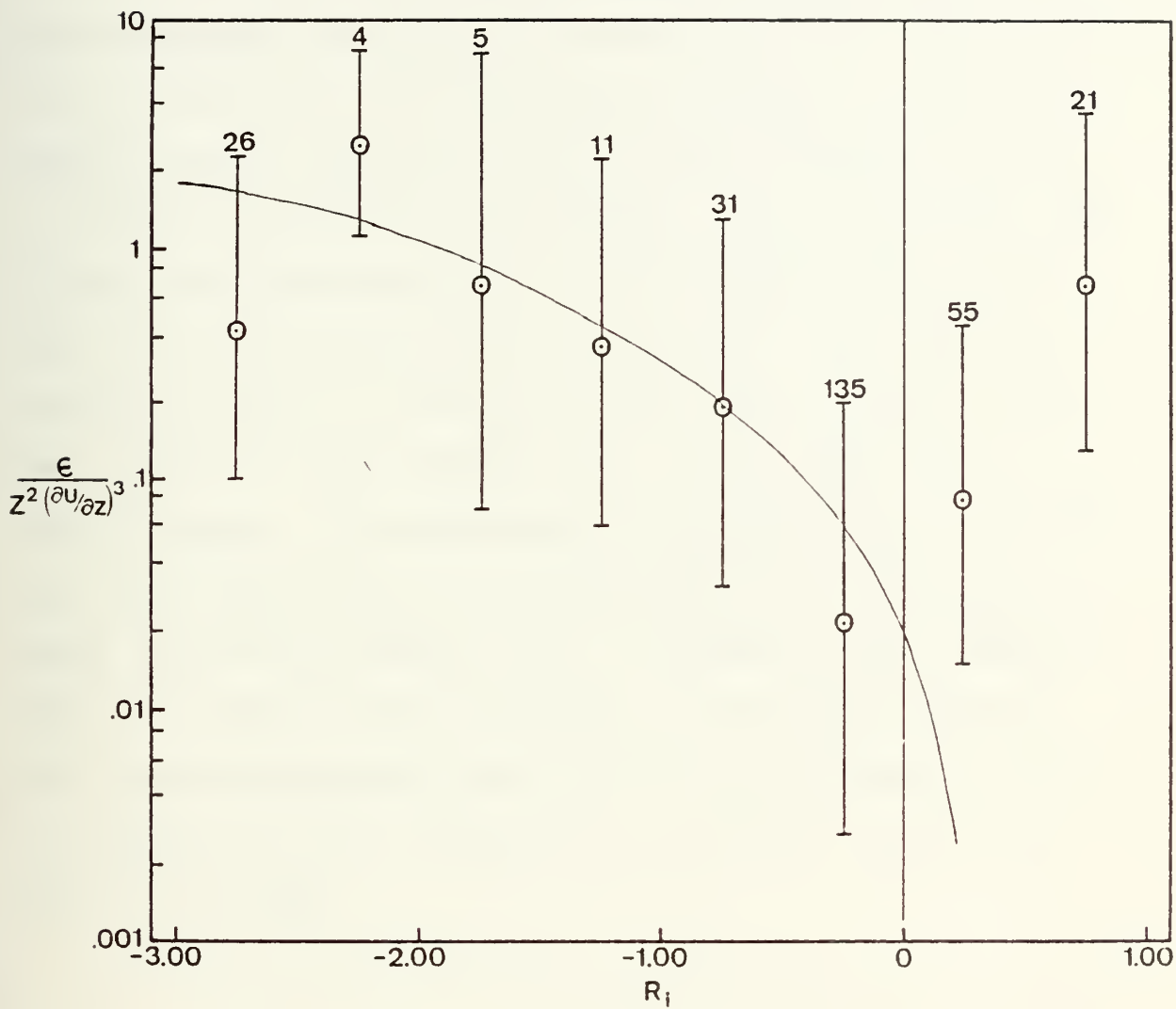


Figure 4. The dimensionless dissipation rate versus Richardson number.

sensors mounted on ships and stationary platforms at levels six meters and higher above the mean sea surface. In order to detect wave influence on turbulence parameters and to get measurements of optical transmission in the layer adjacent to the waves it was necessary to design a system with sensors located within one meter of the actual sea surface.

Several designs were considered. An initial design was an eight meter mast mounted on a small pontoon type float which was to be towed astern of the ship. This presented problems relative to keeping the mast nearly vertical yet have the float small enough to fit on the after deck of the R/V Acania. An exceptionally long umbilical cord would also have been required so the platform could be towed far enough astern to eliminate ship's influence on the measurements. In view of these problems, a system was selected which could be deployed from the bow of the ship and could be tethered in such a manner as to maintain a position in front of the ship.

III. DATA COLLECTION

A. PLATFORM AND LOCATION

All observations were made aboard the R/V Acania and from a small floating platform tethered to the bow of the ship, while anchored in about 30 fathoms of water off Pt. Pinos in Monterey Bay, Figure 5. Conditions over open ocean differ from land in the effects of wave action on turbulence, in the nature of aerosols and fog, and humidity fluctuations. These conditions could best be obtained far at sea; however, the cost of such activities made it desirable to work near land where the optical propagation experiments could be coincident. Pt. Pinos and other locations along the Monterey Bay shoreline provided very nearly the ideal situations for both the optical and meteorological experiments.

B. FLOATING PLATFORM DESIGN

The final design utilized a small, light weight float, 44 inches wide by 56 inches long by 12 inches thick, made of styrofoam and plywood, to support a ten foot hollow mast, made from an inch and one-quarter mild steel pipe. The mast was mounted on the float with two teflon bearings to allow the mast to turn independently of the float. The platform was then tethered to the ship by passing a steel cable down through the hollow mast and out through the bottom of the

float. A 100 pound lead weight was suspended from the end of the steel cable to give enough rigidity to the cable to maintain the mast in a nearly vertical position. The steel cable was then attached to a 15 foot horizontal bow mounted boom to keep the platform at a position ten feet in front of the ship. To deploy the apparatus, the lead weight suspended from the tether cable was lowered to at least ten feet below the float to allow for vertical movement of the float as it followed the wave surface. The float was designed with enough excess buoyancy so that it would follow the wave surface with very little, if any, lag in response.

Two sensor levels were on the vertical mast, one at one meter and another at three meters above the water. A wind vane was also fixed to the mast to keep all the sensors pointed into the wind. A third sensor level was on the horizontal boom above the float approximately seven meters above the water. The umbilical cord ran out along the horizontal boom and then to the top of the mast. A large loop maintained in the cord allowed for vertical displacement of the float. A small hand winch mounted on the horizontal boom was used to lift the entire platform with the steel cable, so it could be swung over the side for easy deployment.

Initial dockside tests were successful and only minor difficulties were encountered when the sensors were mounted. Initially, a rudder was used to keep the float from spinning, but this interfered with the sea-surface temperature probe. As a final modification, the rudder was removed and a small

wind vane was mounted on the float. This kept the float from spinning due to wave action, and in addition reduced the frictional drag on the mast bearings allowing the mast wind vane to keep the sensors more closely aligned with the wind direction.

Photographs on the following pages show the platform, with all sensors mounted in place, being deployed from the bow of the R/V Acania with the ship tied alongside the Coast Guard Pier in Monterey, California. There was no wind or wave action at the time. The platform is always deployed while the ship is at anchor. However, the platform could be deployed underway, at slow speeds, if the float were streamlined, and a streamlined, heavier lead weight were used.

C. INSTRUMENTATION AND PROCESSING EQUIPMENT

Figure 8 shows positions of the instrumentation, cable runs, and processing and recording equipment locations.

The mean wind measurements were obtained with cup anemometer wind profile register systems. The anemometer consists of three cups, plastic cones reinforced with aluminum frames. When the cups rotate a slotted shaft in the anemometer serves as a shutter between a light source and a photoelectric cell. The anemometers have a small amount of internal friction.

Velocity fluctuation measurements were obtained with hot wire anemometer probes with sliding support shields and tungsten wires. The shields permitted isolation of the sensing area for the determination of the undisturbed velocity, V_0 , voltage reading before and after each experiment. The



Figure 6. Photograph of floating platform deployed from the bow of the R/V Acania.

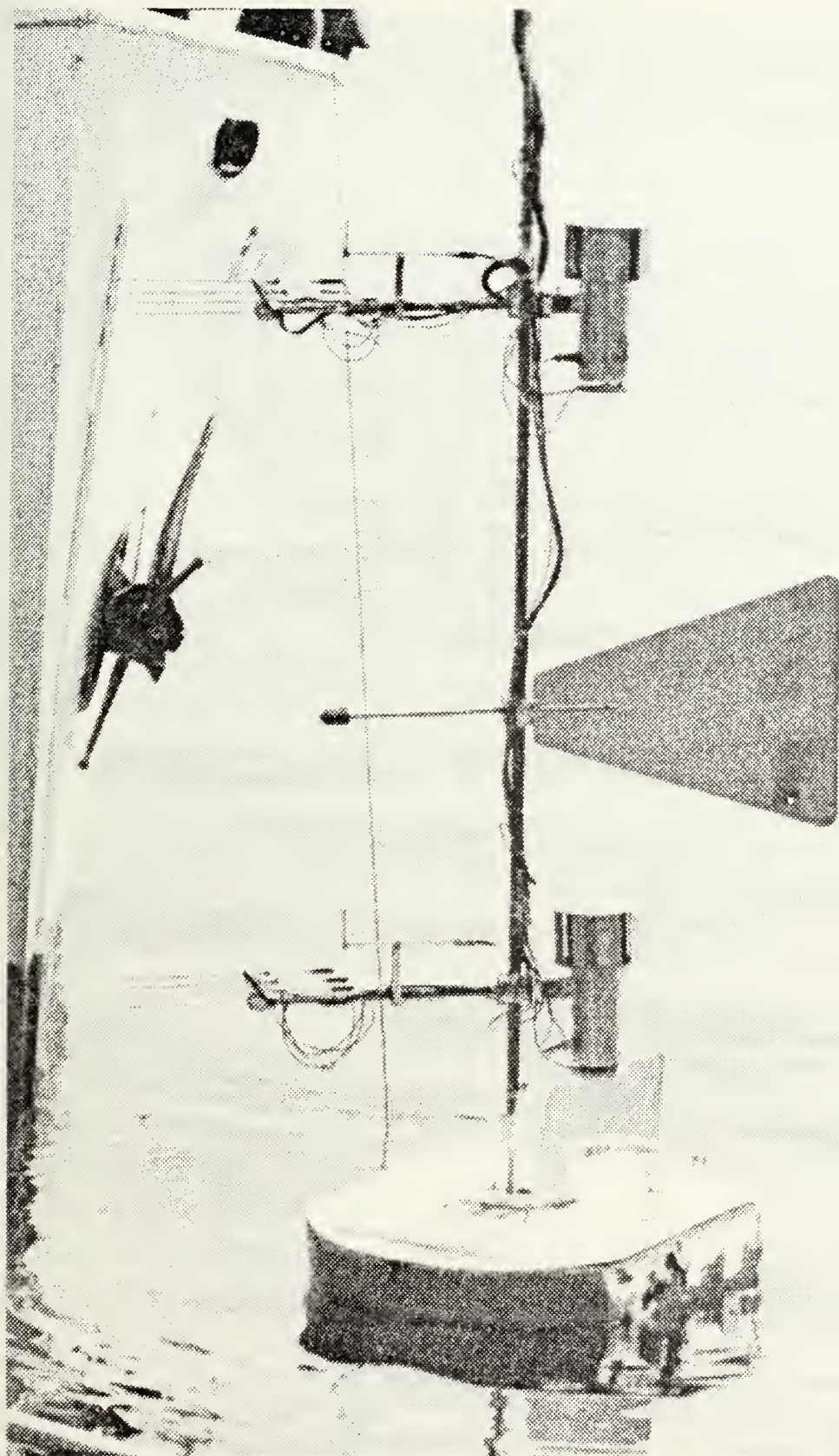


Figure 7. Photograph of sensor arrangement on floating platform.

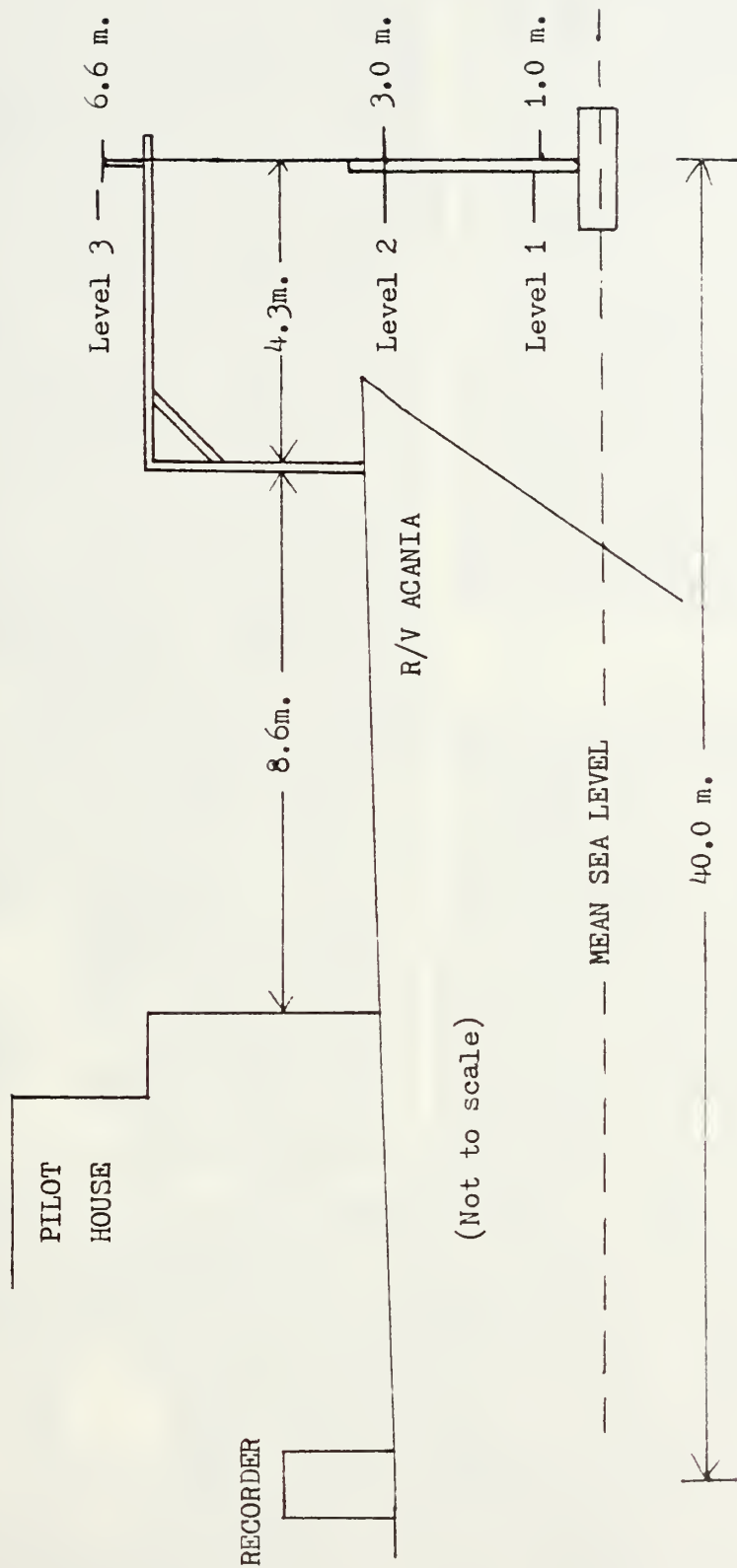


Figure 8. Sensor and instrumentation location on the R/V Acania.

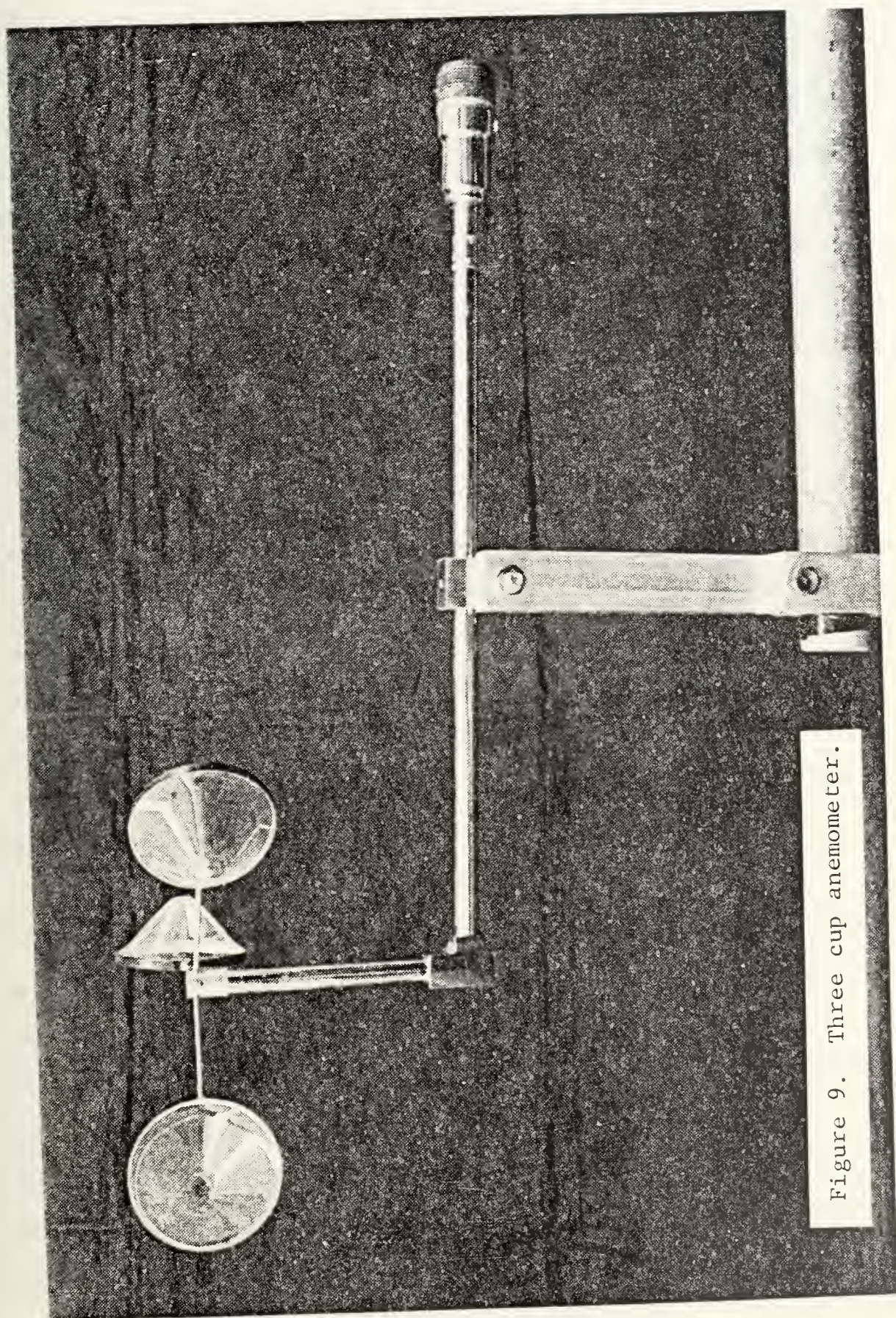


Figure 9. Three cup anemometer.

platinum coated tungsten wire was small enough to resolve the viscous dissipation scale without making corrections for wire length. The anemometer had a linear frequency response from 0 KHz (D.C.) to 10 KHz and the variable decade module operated with a 0-60 ohm range.

Temperature fluctuations were measured using similar size sensors. A platinum wire was used in place of a tungsten wire. The temperature fluctuation system was designed for a resolution of 0.001°C at frequencies up to 1 KHz. The temperature measurements require a bridge circuit.

The baseband portion of this bridge circuit is basically a balanced wheatstone bridge excited by a 3 KHz signal with a synchronous detector on the output. The very small diameter platinum wire serves as temperature sensors in opposite arms of the bridge. The resistance temperature coefficients result in an output from the bridge which is proportional to the temperature difference between the two probes. The sensor wire is 0.5 centimeters long and 2.5×10^{-4} centimeters in diameter. This extremely small mass allows a response to temperature variations of up to 1 KHz, while electronic amplification allows temperature differences as small as 0.004°C to be observed.

Both wind and temperature fluctuation data were recorded on a 14 channel tape recorder. Real time readout on an eight channel chart recorder was used to check the quality of the signals coming from the sensors. The chart data was also utilized in temperature variance analyses.

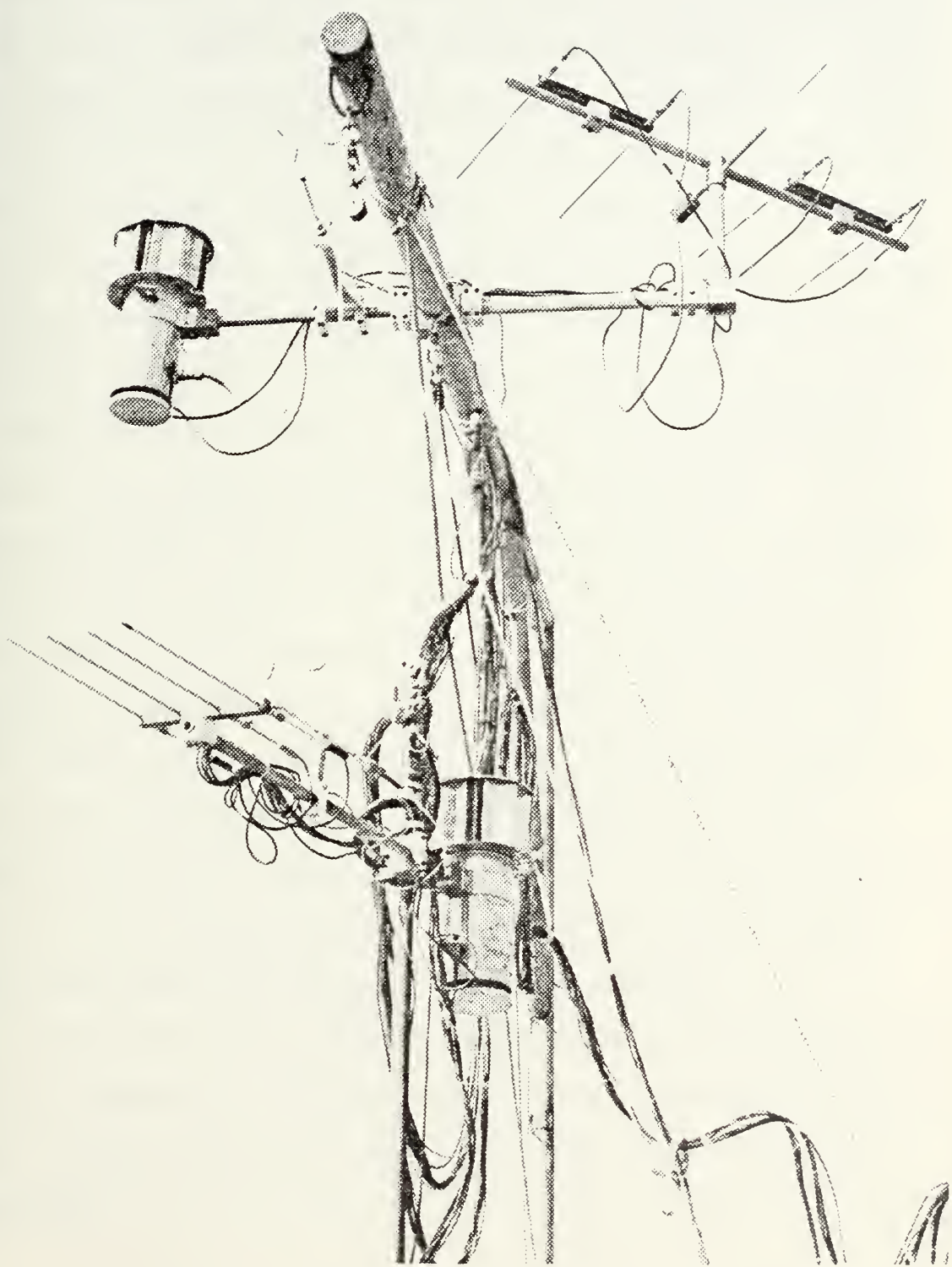


Figure 10. Sensor arrangement at one level.

Temperature sensitive quartz crystal probes were used to obtain mean temperature at the sea surface and four tower levels, Figure 11. The RF signal from the probes and a reference oscillator were mixed in a readout unit to produce a beat frequency whose signature can be analyzed to within $0.001^{\circ}\text{C}/\text{Hz}$. Each sensor received pre-experiment calibration against a platinum resistance wire thermometer in a temperature controlled circulating water bath. It was checked over the range of expected temperatures. The accuracy in achieving a 0.005°C correction factor was a constant for each probe. The tower mounted sensors were housed in aspirated shelters to eliminate radiation effects, Figure 12.

Mean relative humidity information was obtained using Dunmore type lithium chloride sensors, Figure 13. This sensor was also placed in the aspirated shelter. The basic principle of operation of this sensor is resistance change in an electrolytic solution generating a reference voltage variation proportional to relative humidity change. Automatic temperature compensation in the instruments meet the following specifications for relative humidity, $\pm 3\%$ humidity below 90% and $\pm 4\%$ humidity above 90%. Sensor calibration was accomplished by a comparative method using a saturated saline solution in a closed container.

Sensor placement required exceptionally long cable runs, so adjustments were made in the bridges for resistance and capacitance of the wire length to insure good frequency response.

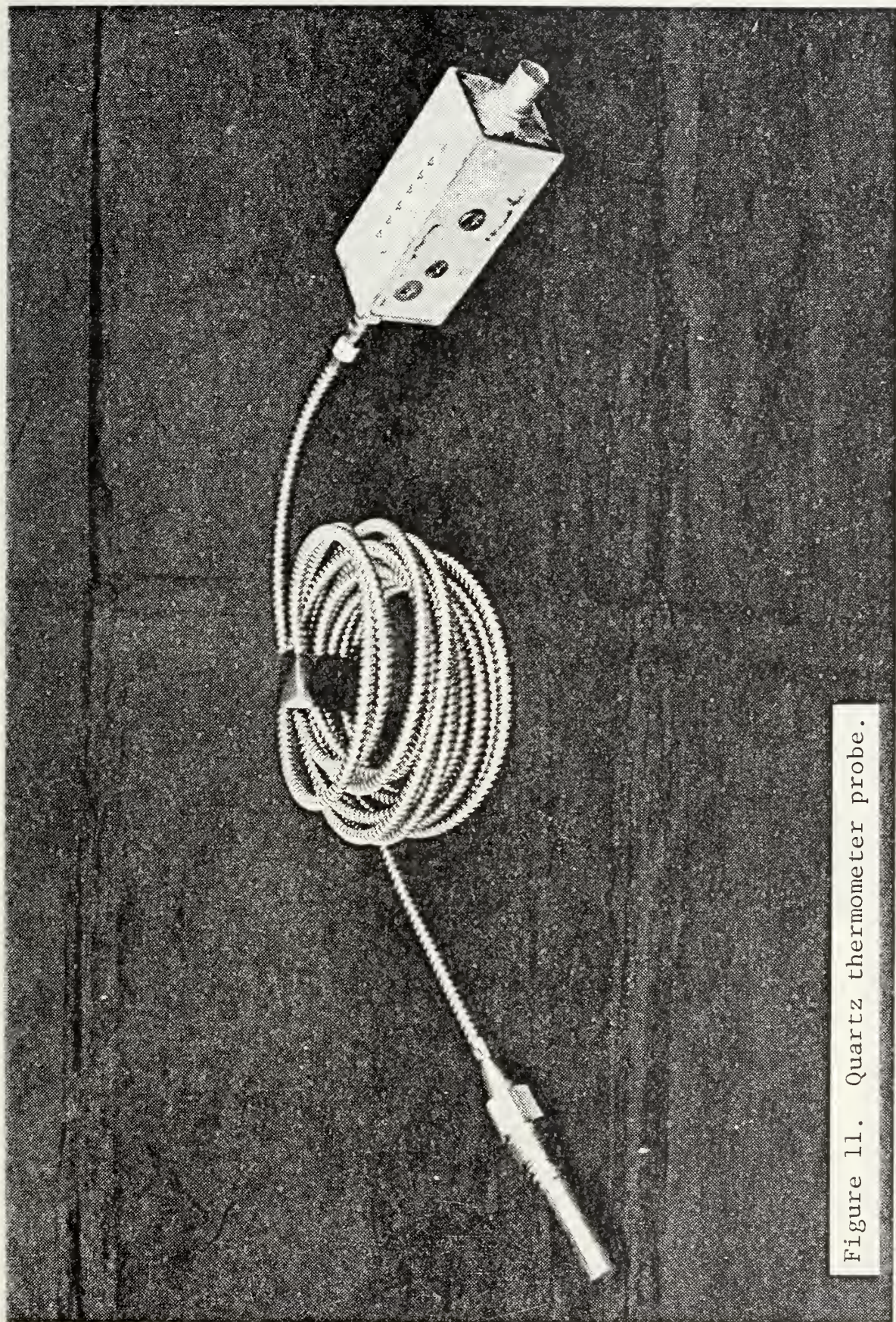


Figure 11. Quartz thermometer probe.

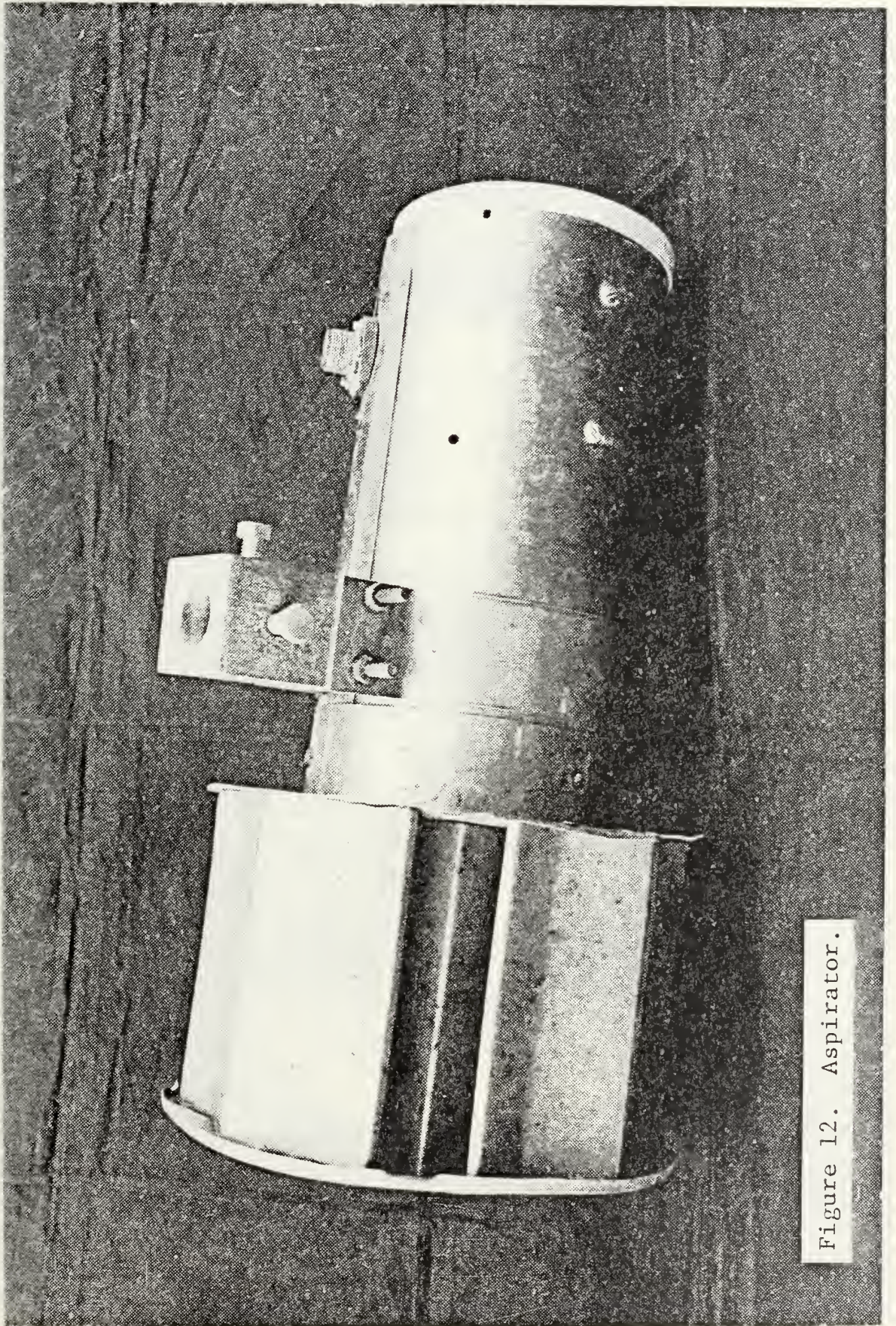


Figure 12. Aspirator.

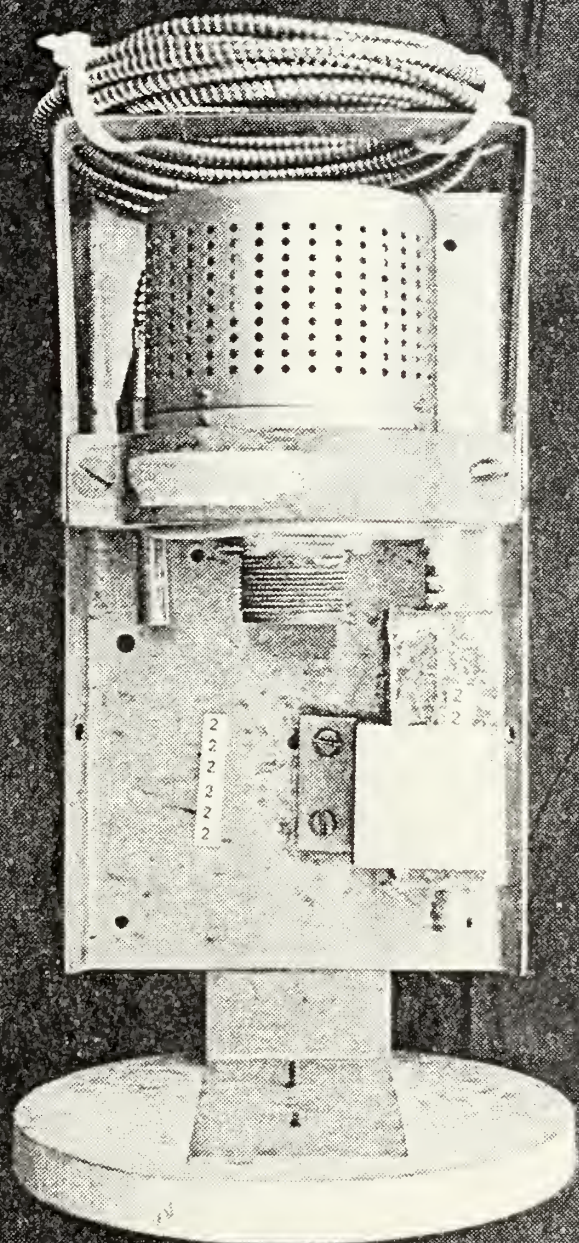


Figure 13. Lithium chloride humidity sensor.

Data logging during the experiments was accomplished using the NPS developed MIDAS (Microprogrammable Integrated Acquisition System). This micro-processor based data acquisition system utilizes an Intel 8008 central processor to control the sampling, averaging, and recording of mean meteorological data. All software is written in PL/M to facilitate the writing of a self-documenting program.

The system is fully automated to sample the tailored list of sensors every 30 seconds and periodically print output values averaged over the selected interval of from one minute to one hour. In this study a ten minute averaging interval was used. Output values were printed out on the teletype in a columnized format with the time of print as a leader. A paper punch was also utilized to produce data cards for use with the IBM 360 digital computer.

IV. ANALYSES PROCEDURES

A. ANALYSES OF MEAN DATA

Analyses were performed on data recorded on teletype printout which was controlled by MIDAS. The data was edited for gross errors or inconsistencies due to known instrumentation malfunctions. The criteria for retaining or discarding data from individual levels or for entire ten minute interval depended on performance check results obtained during measurements, obvious inconsistencies between levels and sequential times, and the availability of fluctuation data. After mean data were obtained for ten minute intervals and passed preliminary editing for obvious erroneous values, it was processed for three applications, i.e., mean wind \bar{U} , mean temperature \bar{T} , and mean humidity \bar{q} . These values were plotted on 2-cycle logarithmic paper. Since \bar{U} , \bar{T} , and \bar{q} are expected to vary logarithmically with height, a best fit straight line should describe the distribution of data points. Best fit lines were used to estimate gradient parameters and the Richardson number.

In general, the procedures were subjective and in some instances, best fit lines with different slopes could be visualized for a given set of data points. Therefore, one criterion used was not to give a single data point too much influence in determining the best fit line. Consequently,

the line drawn represented a most probable position between data points without necessarily coinciding with any point.

B. ANALYSES OF PAIRED TEMPERATURE SENSOR

C_T^2 values were estimated by using paired sensors and variance analyses. This analysis was based on the expression for the temperature structure function, equation (3).

The analysis is one in which temperature differences between paired resistance wires separated by a distance r is subjected to variance analyses as indicated by the term $[T'(x) - T'(x+r)]^2$ on equation (3).

Voltages corresponding to the temperature differences, ΔT , as measured by the paired sensors were recorded on analog magnetic tape. During experimental periods, calibration voltages were also recorded on the data tape for reconstruction of the signal. This calibration signal was played back at the time of data analysis to provide a reliable check of the recording system performance in both record and playback modes.

The variance or mean square of the temperature differences required to compute C_T^2 was obtained by analyzing the analog voltages with a mean square voltmeter using a 30 second time constant for the averaging. The output of the mean square voltmeter as well as a record of the original signal were recorded on standard strip charts. A strip chart section appears in Figure 14. The record of the original instantaneous signal provides an important means of spotting extraneous noises. The rms voltmeter-strip chart recorder

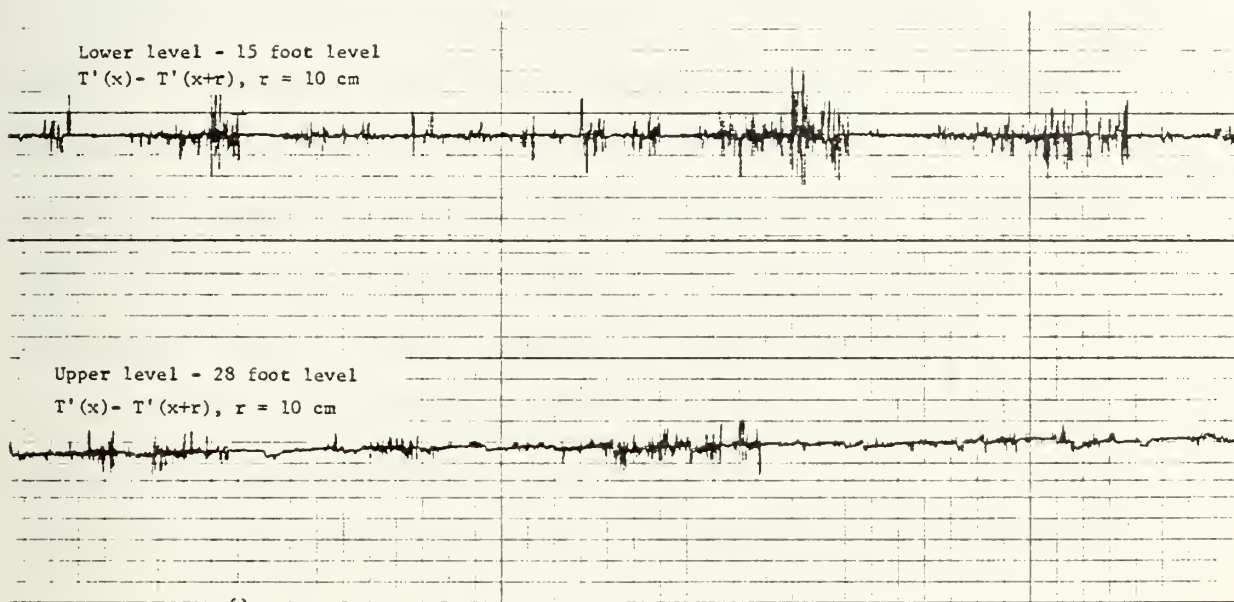


Figure 14. Example of strip chart section.

system was also calibrated using known input voltages. At least one input calibration voltage was larger than the largest expected signal on the data record and likewise one input calibration voltage was lower than the smallest expected signal. This procedure minimized any non-linearities in either the rms or the strip chart recorder.

A final check on the validity of the measured data was made by performing spectral analyses on a few representative data samples from each experimental run. The spectrum analyzer, described in section C, was used to obtain the spectra which were subsequently plotted and kept as a permanent record. Any harmonic noise appeared as a spike in an otherwise reasonably smooth curve. It should be emphasized that continuous calibration and data checking procedure were essential steps throughout the analyses.

C. ANALYSES OF VELOCITY FLUCTUATION DATA

Spectral analyses to obtain ϵ values were performed on fluctuating velocity data obtained with single wires oriented in the vertical normal to the mean wind. These data represent a point measurement and yield temporal or time descriptions of the fluctuations. Twenty-one minute segments of data originally recorded on magnetic tape were recorded into a digital spectrum analyzer. Procedures for converting spectral values, obtained with the analog spectral analyzer, to engineering units and for obtaining turbulence parameters from the spectra are described in the following paragraphs.

A necessary procedure was to scale the spectral plots in order to relate rms input voltages to power spectral densities (PSD), variance per unit frequency. To obtain PSD levels, corresponding to rms voltage input, calibrated scale charts were constructed.

Amplitude scaling calibrations were accomplished using externally generated white noise. Signals with a 1 volt rms over a frequency range of 0.1 Hz to 1000 Hz, giving a PSD of $10^{-3} \text{ v}^2/\text{Hz}$. Setting a 3.16 v (10 dB) input gain on the spectrum analyzer insures that 1 volt input corresponds to $Y=0$. An example of such a calibration plot is shown in Figure 15.

ϵ estimates were obtained from the variance spectra on the basis of the universal formulae for the inertial subrange in wave number space. These expressions predict a $-5/3$ slope for variance spectra of both velocity and temperature when plotted in log-log format. Figures 16 and 17 are typical spectra of both variables considered in the analyses. The velocity variance spectra have consistent $-5/3$ slope. However, temperature spectra often exhibited slopes slightly different from the expected value of $-5/3$. This feature of temperature spectra has been observed by others and the existence of "cold spikes" in the temperature traces has been postulated as a probable cause (Friehe, 1976).

Since velocity was measured at a fixed point in the flow, the resultant spectral estimates correspond to "temporal" frequencies, f . To obtain ϵ values, temporal (f) and

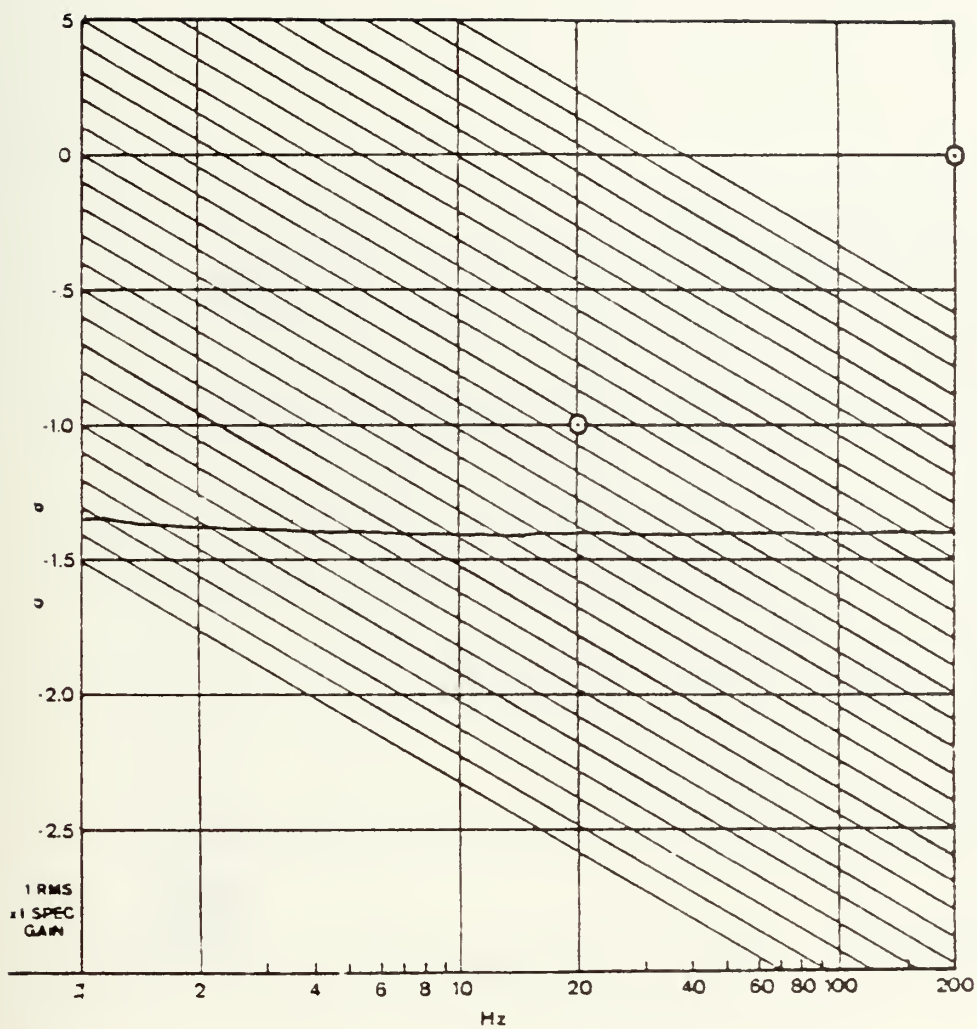


Figure 15. Calibration plot for spectrum analyzer.

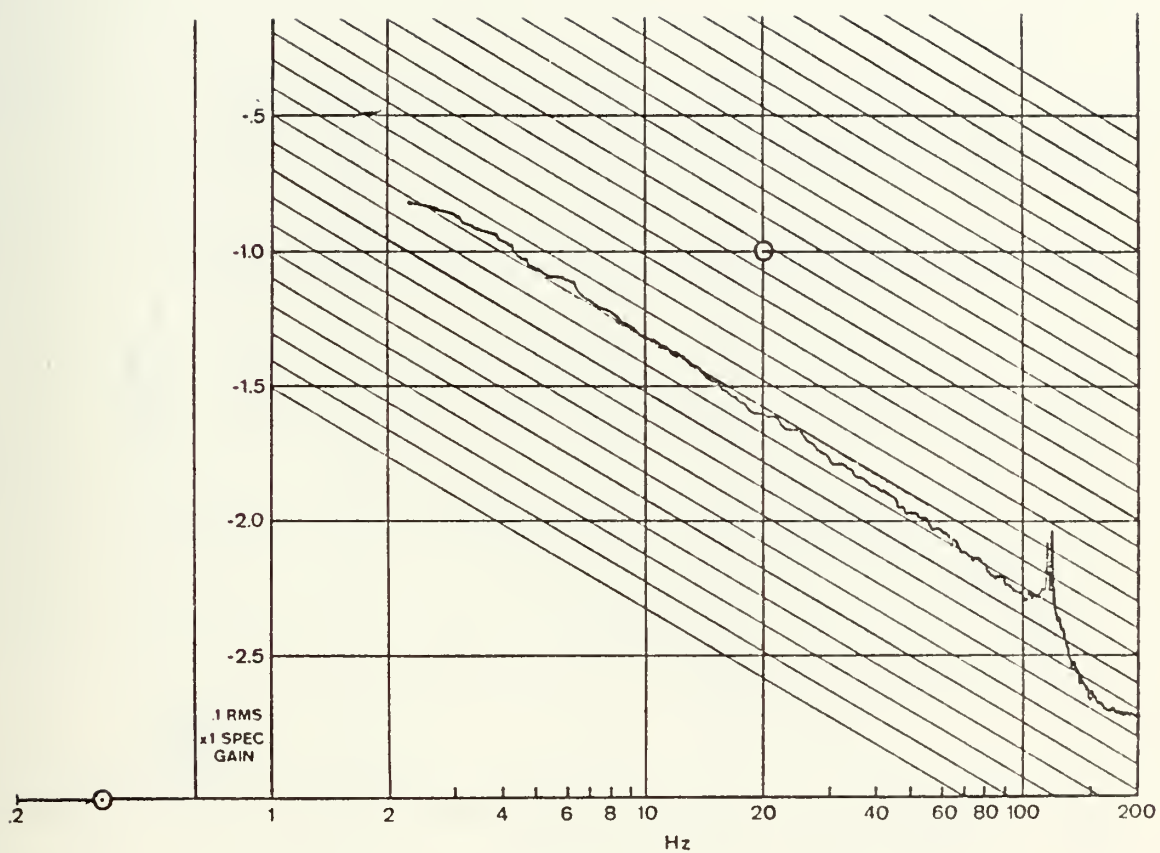


Figure 16. Example of temperature variance spectra.

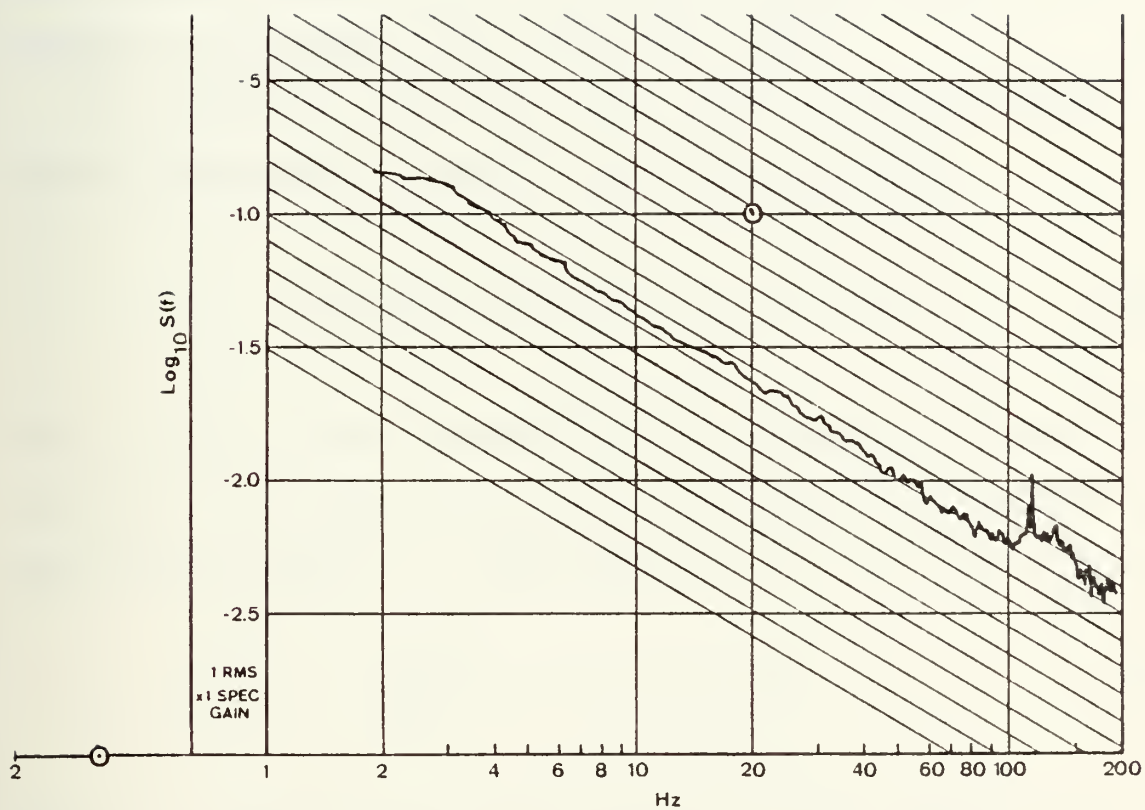


Figure 17. Example of velocity variance spectra.

space (k) scales had to be related. This was accomplished by Taylor's (1938) "frozen turbulence" hypothesis, that is

$$k = 2\pi f/\bar{U} \quad (25)$$

where \bar{U} is the mean wind at the measurement level. The term "frozen" implies the turbulence pattern remains unchanged as it sweeps past the sensor probe.

The following identities were used to relate temporal spectral estimates to spatial spectral estimates

$$f \cdot S_u(f) \equiv k \cdot S_u(k) = C_1 \epsilon^{2/3} k^{-2/3} \quad (26)$$

where $S_u(f)$ is the spectral density value with units of $(\text{m/s})^2/\text{Hz}$. The above equation is rewritten in the following form to obtain ϵ from values of f , \bar{U} , and $S_u(f)$.

$$\epsilon = \left\{ \frac{k^{2/3}}{C_1} \cdot f \cdot S_u(f) \right\}^{3/2} \quad (27)$$

where $k = 2\pi f/\bar{U}$ and $C_1 = .5$ and $C_2 = .25$, empirically.

D. TEMPERATURE SENSOR AND HOT WIRE CALIBRATION

In-situ calibrations of the velocity sensors were performed every 10 minutes during the experiment. For this, recordings were made of both the cup anemometer wind speed and the corresponding hot wire voltage output. The voltage from the sensor is given by

$$V^2 = a \bar{U}^{1/2} + b \quad (28)$$

where V is the hot-wire voltage output and \bar{U} is the mean wind speed for any given level. The constants, a and b , are the calibration curve slope and intercept respectively, and were derived from the in-situ calibration curve.

To convert the voltages to velocity units requires a calibration factor given by

$$U' = Cv' \quad (29)$$

where C is the calibration factor in m/s /volt. v' is the voltage fluctuation, and U' the velocity fluctuation. Differentiating equation (28) yields

$$U' = (4vU^{\frac{1}{2}}/a) v' \quad (30)$$

which when substituted into equation (27) yields

$$C = 4vU^{\frac{1}{2}}/a \quad (31)$$

An example in-situ calibration curve is shown in Figure 15. The slope of the curve yields the value for " a " in equation (31).

V. RESULTS

Results are multi-level mean estimates of C_N^2 (derived from C_T^2) and ϵ . An immediate concern in interpretation was the possible influence of the ship's structure on the measured parameters. The absence of any strong ship influence can be established, however. In Figure 18 are typical profiles of the mean wind data obtained during this experiment. The mean wind versus height is plotted on a log-linear scale producing a straight line, which is to be expected in the neutral case. The agreement with the neutral case prediction for the mean wind profiles suggests that the ship influence on all levels was negligible. Other evidence that the ship influence was not a factor in observed results will be presented in the discussion of C_N^2 and ϵ results which follows.

It had originally been planned to obtain wave spectra data for use in determining the swell wave speeds in the analyses. However, the accelerometer attached to mast on the floating platform did not function properly, and no usable interpretation based on observed wave data is possible.

C_N^2 (or C_T^2) Results

The primary interest in this study was to examine the height variation of the optical parameter C_N^2 . During the entire data collection period the stability was stable or

2/16/77

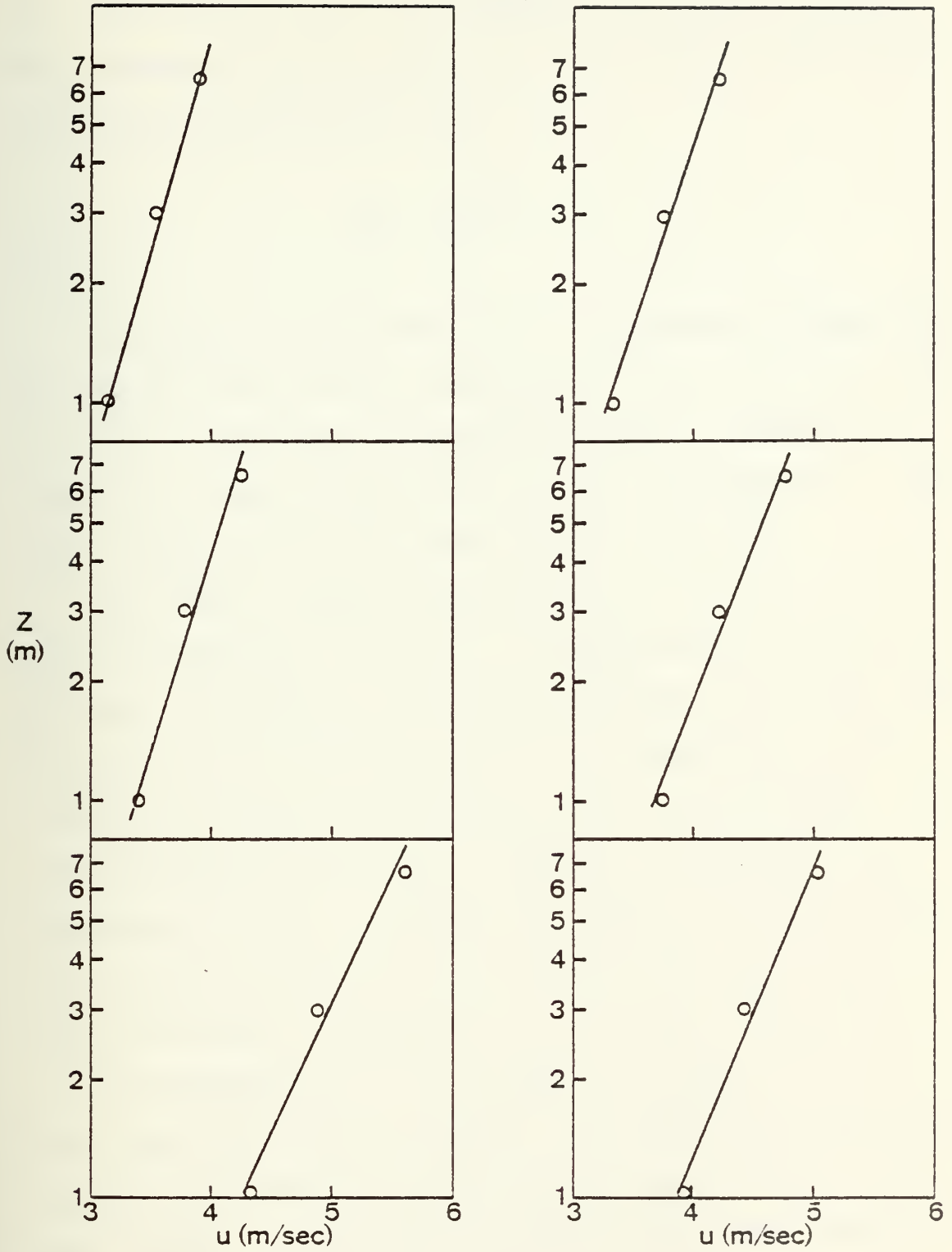


Figure 18. Example plots of mean wind versus height.

very near neutral. For near neutral conditions, neglecting the wave influence, Equation (11) predicts the following height dependence for C_N^2 ,

$$C_N^2 \propto Z^{-2/3}$$

In Figure 19 are results of this experiment along with the results from earlier experiments. The latter are shown in order to emphasize the possible slopes. A best fit line to the upper three levels closely approximates a $-3/2$ slope, agreeing with the near neutral prediction.

The previous examination of results did not take the wave influence into account. In observational studies of the wave influence on turbulence parameters, Davidson (1974) observed the wave influence to be as significant as the stability influence as the sea surface is approached. This wave influence could have the effect of increasing the turbulence in the air immediately above the waves during near neutral conditions and thus increasing C_T^2 and C_N^2 above the waves as compared to over a flat sea surface.

A re-examination of the results in Figure 19 at the 6.6 meter level and below, indicates that the wave influence is evident by a marked increase in C_N^2 values at the 3 and 1 meter levels. Even though conditions were near neutral, the profile of the lower three points approaches the relationship for the unstable case

$$C_N^2 \propto Z^{-4/3}$$

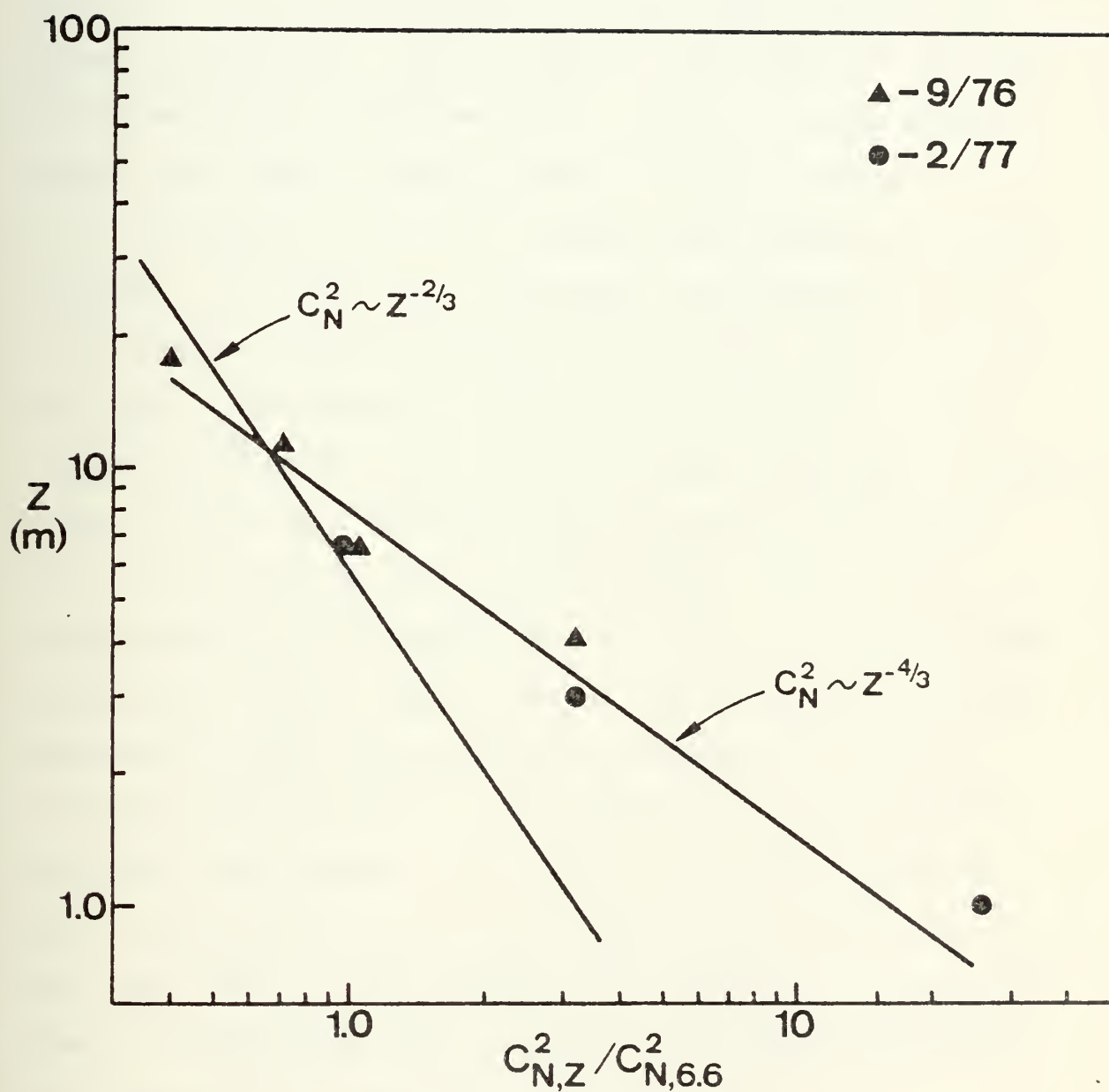


Figure 19. Normalized C_N^2 (computed from C_T^2) results versus height.

Qualitatively, this is an indication that the wave influence very near the sea surface may override the stability effect, especially on C_T^2 and C_N^2 .

Wave influence is also evident in the near neutral portion ($Ri \approx 0$) of the summary of lower level results data shown in Figure 20. Here it can be seen that the observed non-dimensional overwater results in general have higher values than those predicted based on only stability.

In addition to the C_N^2 obtained from shipboard meteorological, C_T^2 , data, this experiment was coordinated with a shorebased laser experiment that obtained C_N^2 from optical data. In Figures 21, 22, and 23 are the time variations of C_N^2 at the three levels for this experiment plotted along with the C_N^2 obtained from the optical experiment. The results labeled MTF are from optical data and the results BUS are from meteorological data at the shore based laser site. These results have a much closer correlation between the shore based optically obtained C_N^2 and the shipboard meteorologically obtained C_N^2 than previous experiments have shown. This closer correlation could be due to the fact that data was taken at this low level, which was very near the mean height above the waves of the laser beam's transmission path. Previous shipboard measurements were made at 6.6 meters and higher.

ϵ and U_* Results

Figure 24 is a plot of the normalized ϵ results versus height. Again, data from this experiment is coupled to data

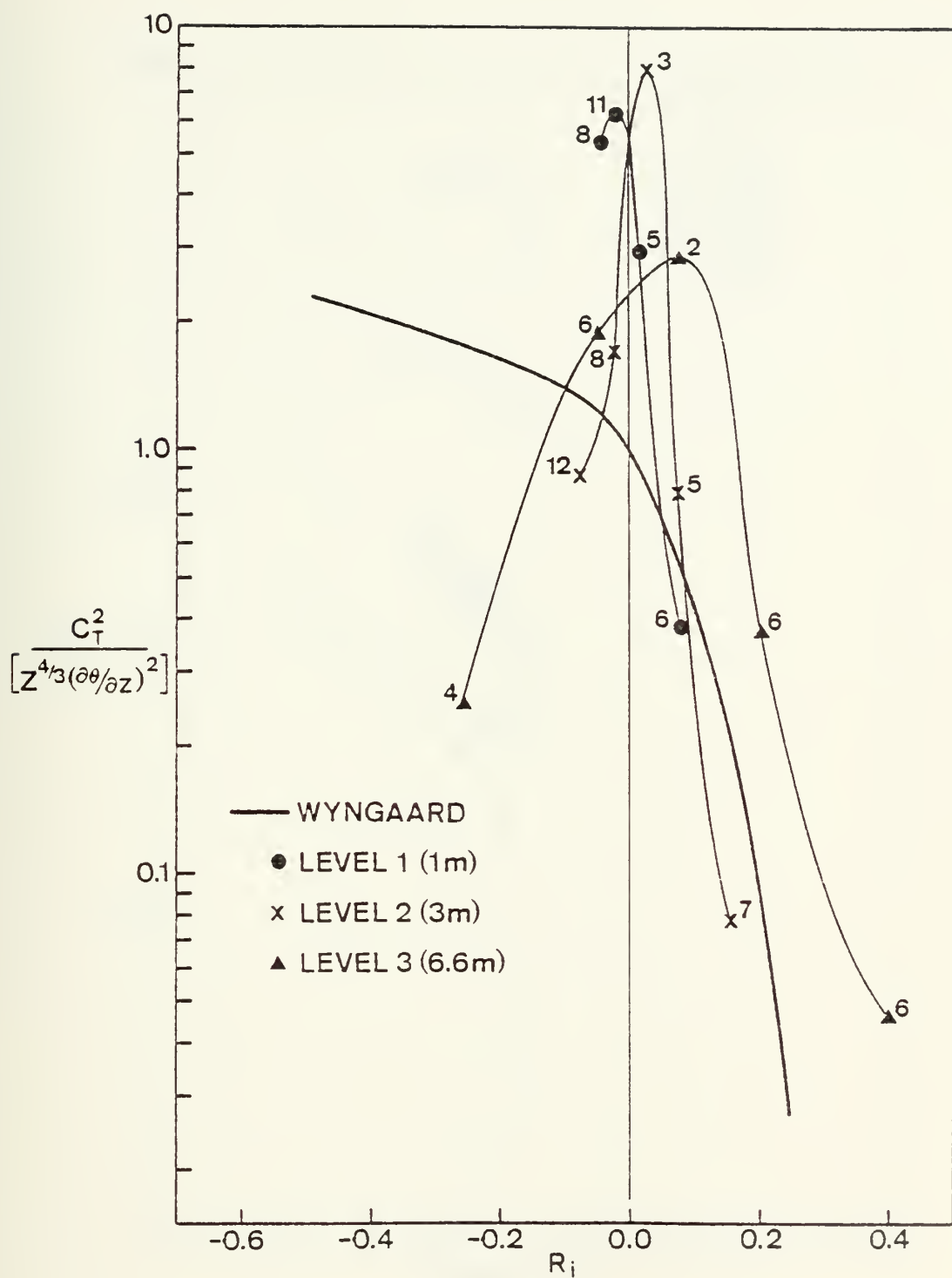


Figure 20. Summary of results of low level DTSFP versus Richardson number.

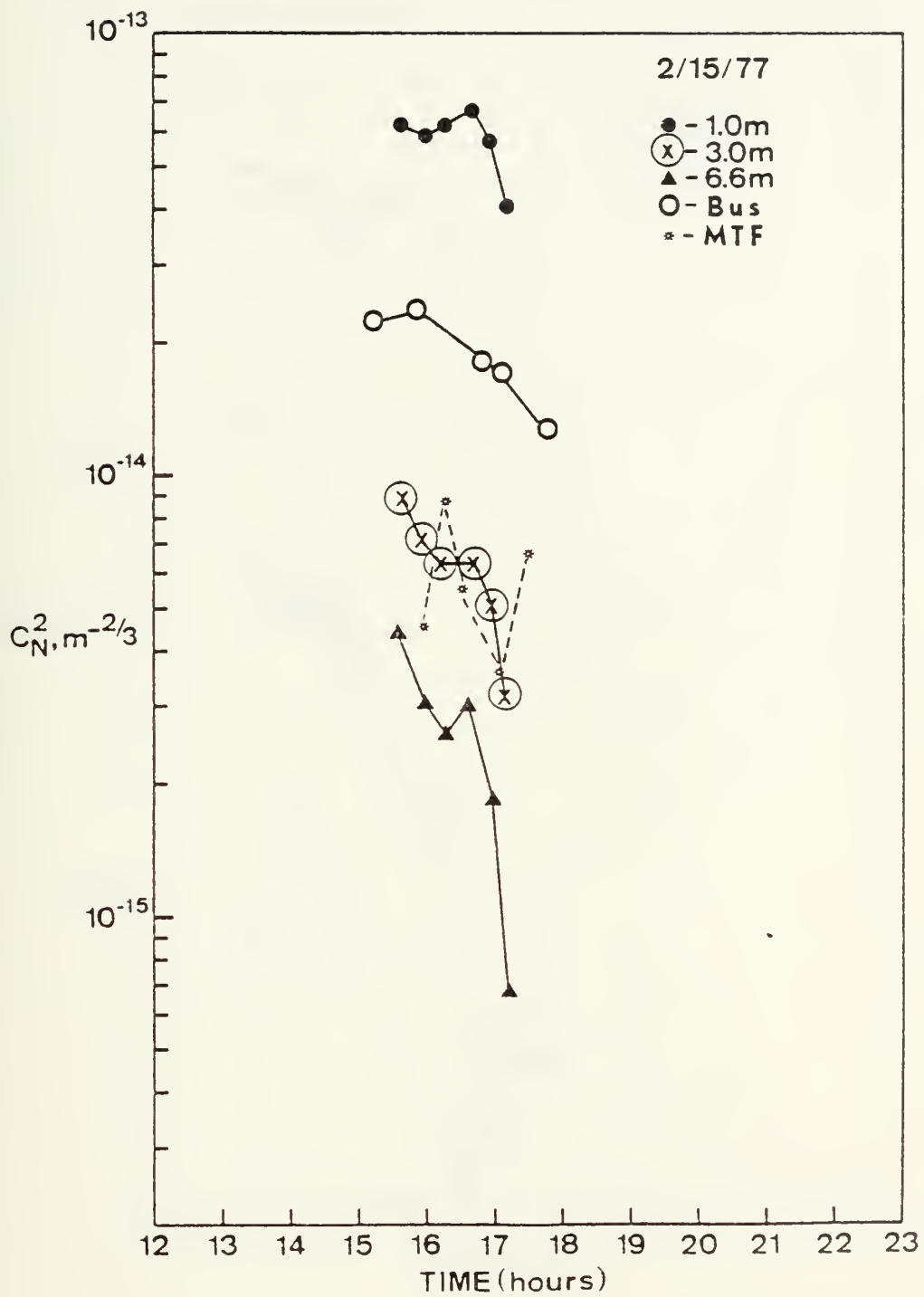


Figure 21. C_N^2 versus time - shipboard results compared to shore results for 2/15/77.

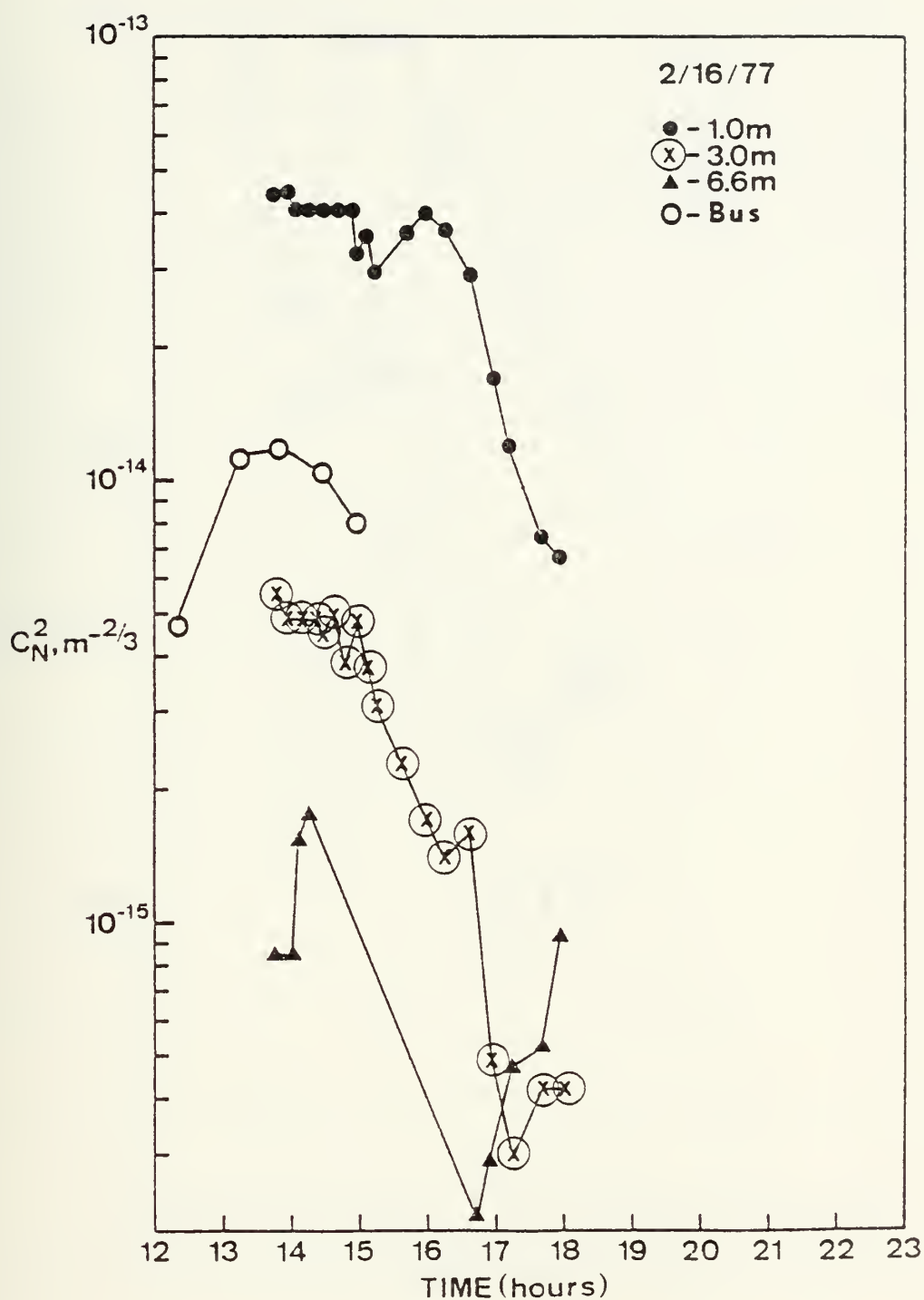


Figure 22. C_N^2 versus time - shipboard results compared to shore results for 2/16/77.

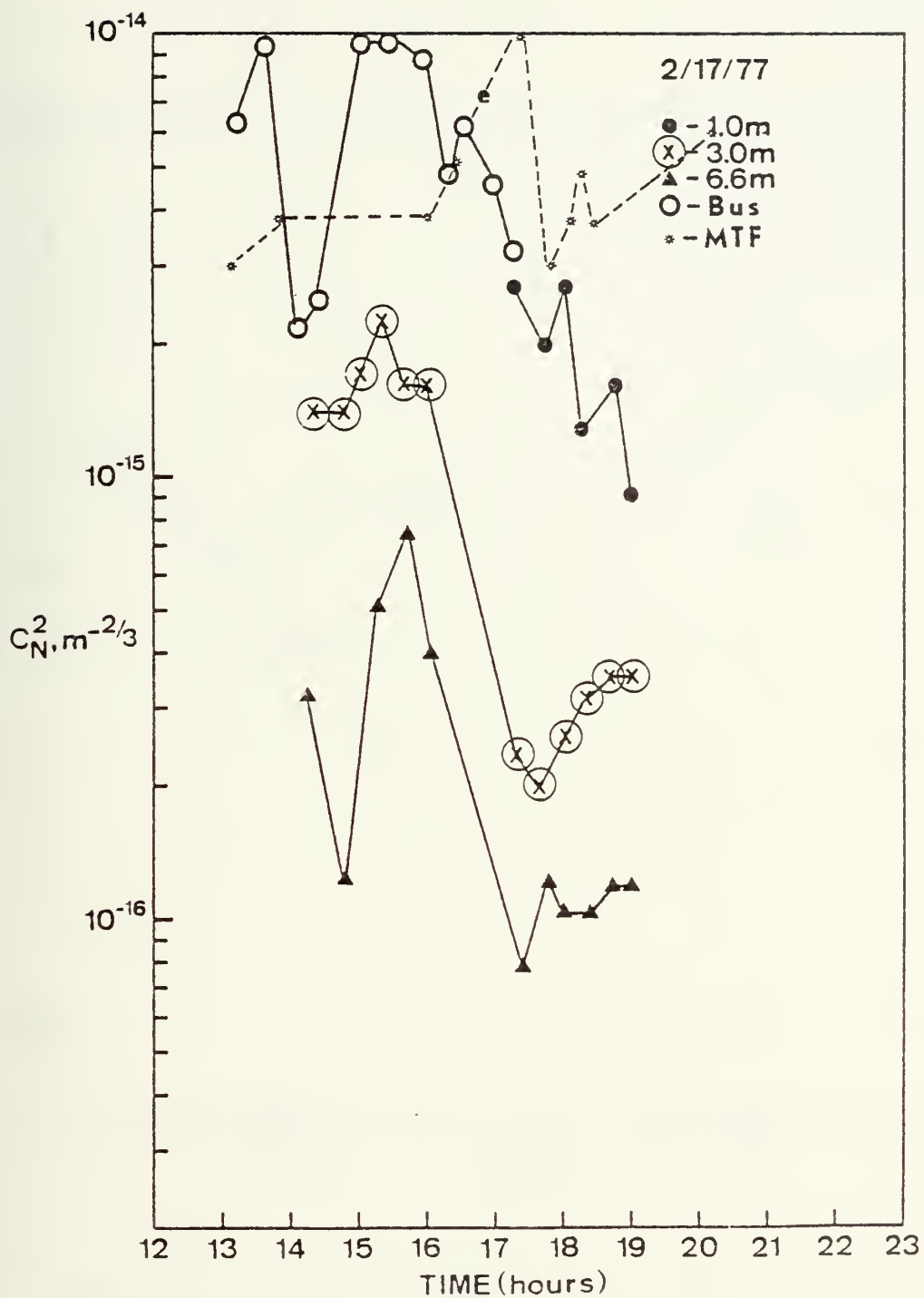


Figure 23. C_N^2 versus time - shipboard results compared to shore results for 2/17/77.

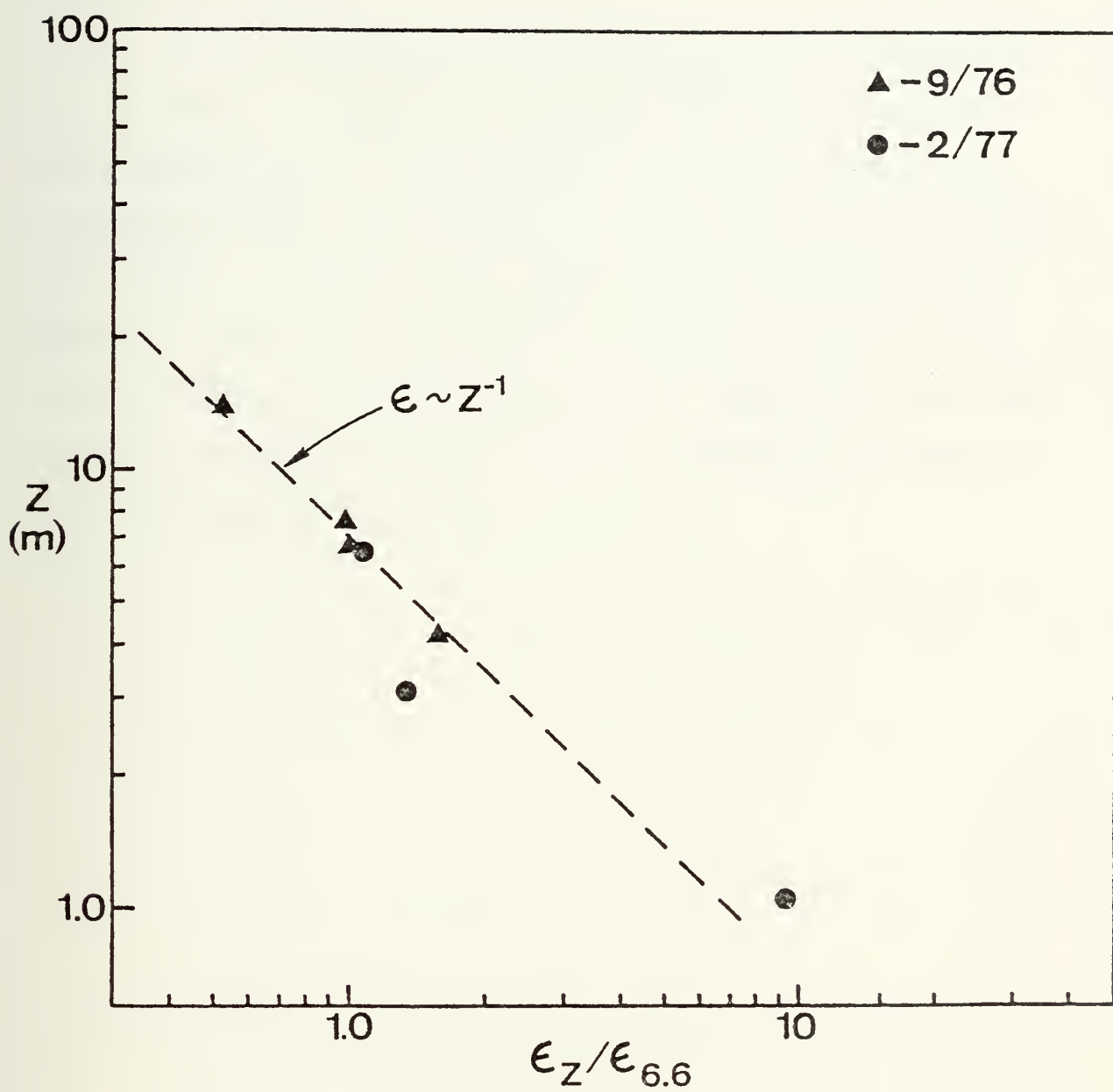


Figure 24. Normalized dissipation rate ϵ versus height.

from earlier experiments to emphasize the slope. Except for the three meter level value, the mean profile describes the predicted -1 slope.

U_* results for this experiment are shown in Figure 25. U_* is plotted for each level that dissipation (ϵ) data was available and is also shown for profile ($\partial U / \partial Z$) data. An assumption for the surface layer is that U_* is constant with height. These results support this assumption, in general, since U_* values at any given time appear to be within a factor of two of one another. Results in the small table in the upper right hand corner of Figure 25 indicate that the mean values are quite close.

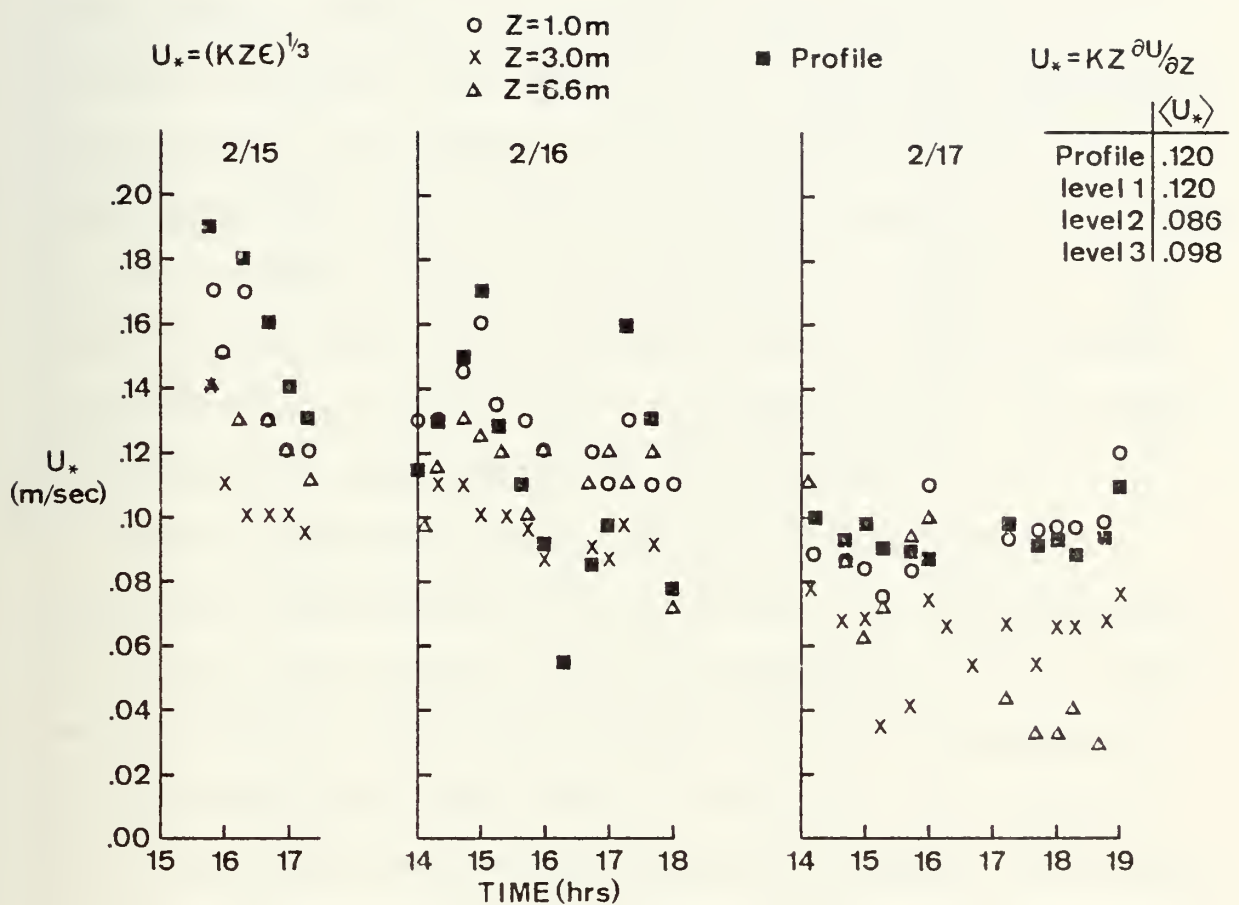


Figure 25. Plots of U_* versus height for each level and table of comparison of the means.

VI. CONCLUSIONS

The purpose of this study was to use previously developed relationships, based on recognized sound principles, to validate procedures for measuring the turbulence parameters very near the sea surface. The experimental results do agree reasonably well with the predicted results, substantiating the validity of the new procedures. In addition, the results showed very clear evidence that the wave influence is prominent in the very near sea surface layer. It could be as important a consideration as the stability.

There is more development needed to formulate the theoretical relationships which indicate the wave influence on the near sea surface turbulence parameters. This experiment provided a viable and reliable method for collecting the necessary data from a ship. The use of the tethered floating platform allows expanded use of already proven data collection procedures and instrumentation, thus accomplishing the primary objectives of this study.

APPENDIX A

DATA TABLES

TABLE I

DAY	TIME	TEMPERATURE °C				WIND SPEED M/SEC		
		T _s	T ₁	T ₂	T ₃	U ₁	U ₂	U ₃
2/15/77	1540	14.45	15.14	15.20	15.25	3.83	----	5.10
"	1600	-----	-----	-----	-----	-----	-----	-----
"	1620	14.35	15.23	15.37	15.49	3.61	----	4.78
"	1640	13.84	15.10	15.28	15.44	3.24	----	4.32
"	1700	13.96	14.84	15.06	15.25	2.95	----	3.85
"	1720	14.03	14.56	14.76	14.93	2.95	----	3.81
2/16/77	1350	13.38	12.93	12.77	12.59	3.00	----	3.73
"	1400	13.28	12.82	12.67	12.52	3.15	3.51	3.93
"	1410	13.25	12.47	12.34	12.19	3.34	3.73	4.22
"	1420	13.23	12.29	12.15	12.00	3.39	3.76	4.24
"	1430	13.19	12.21	12.08	11.94	3.29	3.71	4.20
"	1440	13.16	12.23	12.12	11.97	3.76	4.22	4.76
"	1450	13.13	12.17	12.07	11.95	4.32	4.88	5.61
"	1500	13.11	12.12	12.02	11.91	3.95	4.42	5.05
"	1510	13.08	12.06	11.96	11.85	3.78	4.12	4.73
"	1520	13.07	12.06	11.97	11.87	3.29	3.71	4.05
"	1540	13.03	12.03	11.94	11.83	3.00	3.24	3.73
"	1600	13.00	11.93	11.85	11.75	2.73	3.00	3.34
"	1620	12.90	11.96	11.87	11.77	2.41	2.68	2.93
"	1640	12.95	12.11	12.04	11.95	2.51	2.76	3.07
"	1700	12.94	12.29	12.23	12.15	2.78	3.07	3.44
"	1720	12.98	12.45	12.40	12.34	2.78	3.39	3.83
"	1740	12.98	12.49	12.43	12.35	3.17	3.44	4.07
"	1800	12.89	12.53	12.53	12.52	2.24	2.46	2.71
2/17/77	1420	13.25	14.83	14.79	14.73	2.15	2.46	2.81
"	1440	13.28	14.82	14.77	14.71	2.00	2.27	2.61
"	1500	13.45	14.88	14.88	14.86	1.68	1.98	2.34
"	1520	13.45	15.02	15.02	15.01	1.68	1.93	2.29
"	1540	13.45	15.33	15.36	15.38	1.90	2.12	2.51
"	1600	13.51	15.27	15.23	15.20	1.93	2.22	2.51
"	-----	-----	-----	-----	-----	-----	-----	-----
"	1720	13.26	14.65	14.68	14.69	1.68	1.98	2.34
"	1740	13.30	14.14	14.22	14.29	1.66	1.98	2.29
"	1800	13.36	13.82	13.92	14.00	1.18	1.95	2.34
"	1820	13.42	13.72	13.83	13.93	1.73	1.98	2.36
"	1840	13.40	13.63	13.74	13.83	1.73	1.98	2.37
"	1900	13.41	13.66	13.75	13.82	1.95	2.22	2.71

TABLE II

DAY	TIME	RELATIVE HUMIDITY %			SPECIFIC HUMIDITY gm/kg			
		H ₁	H ₂	H ₃	q ₀	q ₁	q ₂	q ₃
2/15/77	1540	72.5	73.3	72.2	10.31	7.81	7.93	7.84
"	1600	-----	-----	-----	-----	-----	-----	-----
"	1620	73.6	71.2	65.2	10.24	7.98	7.79	7.22
"	1640	73.2	70.1	64.8	9.91	7.86	7.63	7.12
"	1700	76.0	71.7	67.9	9.99	8.04	7.69	7.37
"	1720	79.2	74.0	72.1	10.04	8.22	7.87	7.67
2/16/77	1350	85.8	-----	89.6	9.62	8.02	-----	8.19
"	1400	88.8	86.0	91.7	9.56	8.28	7.90	8.34
"	1410	91.2	87.6	93.4	9.54	8.27	7.87	8.31
"	1420	92.9	88.7	94.5	9.53	8.32	7.87	8.36
"	1430	94.1	89.3	95.1	9.50	8.40	7.89	8.32
"	1440	95.1	90.1	95.7	9.48	8.49	7.98	8.40
"	1450	95.4	90.3	96.2	9.47	8.48	7.97	8.43
"	1500	96.4	91.4	97.1	9.45	8.54	8.04	8.48
"	1510	97.4	92.3	97.7	9.43	8.60	8.09	8.50
"	1520	98.1	92.9	98.5	9.43	8.66	8.15	8.58
"	1540	98.6	93.0	99.0	9.40	8.69	8.14	8.60
"	1600	98.7	93.0	99.1	9.39	8.70	8.05	8.57
"	1620	99.5	92.5	99.7	9.33	8.73	8.06	8.63
"	1640	97.6	93.0	-----	9.36	8.54	8.19	-----
"	1700	-----	-----	-----	-----	-----	-----	-----
"	1720	-----	-----	-----	-----	-----	-----	-----
"	1740	-----	93.8	94.0	9.37	-----	8.49	8.46
"	1800	-----	93.5	99.1	9.32	-----	8.51	9.02
2/17/77	1420	71.8	72.3	72.4	9.54	7.59	7.63	7.61
"	1440	75.3	74.0	72.7	9.56	7.96	7.79	7.63
"	1500	75.8	72.8	70.3	9.67	8.04	7.72	7.45
"	1520	73.7	71.2	66.1	9.67	7.89	7.62	7.07
"	1540	70.5	67.5	63.6	9.67	7.70	7.39	6.97
"	1600	72.3	70.0	66.0	9.71	7.86	7.60	7.15
"	1620	-----	-----	-----	-----	-----	-----	-----
"	1720	78.3	78.1	74.7	9.55	8.18	8.20	7.82
"	1740	85.7	84.1	81.0	9.58	8.17	8.55	8.27
"	1800	90.6	88.8	85.0	9.61	8.17	8.85	8.52
"	1820	92.3	89.7	85.7	9.65	9.08	8.89	8.55
"	1840	92.6	90.2	86.3	9.63	9.06	8.89	8.55
"	1900	92.9	90.5	86.6	9.64	9.11	8.92	8.58

TABLE III

DAY	TIME	$C_N 10^{-8} m^{-2/3}$			$\epsilon 10^{-3} m^2/sec^3$			$\partial\theta/\partial Z_{10}$ 10^{-2}	U_* m/sec
		1	2	3	1	2	3		
2/15/77	1540	25.	9.3	6.6	14.0	2.4	1.1	+0.87	.190
"	1600	24.	8.4	5.5	10.0	1.3	1.5	-----	-----
"	1620	25.	7.9	5.1	13.0	1.1	1.0	+1.57	.180
"	1640	26.	7.9	5.5	5.8	1.0	0.92	+2.06	.160
"	1700	24.	7.1	4.3	5.5	1.1	0.74	+2.45	.140
"	1720	20.	5.7	2.6	5.0	0.81	0.63	+2.25	.130
2/16/77	1350	21.	7.4	2.9	5.8	0.49	0.43	-1.50	.110
"	1400	21.	7.0	2.9	6.2	0.49	0.38	-1.30	.120
"	1410	20.	7.0	4.0	6.3	1.0	0.57	-1.19	.130
"	1420	20.	7.0	4.3	6.8	1.7	0.83	-1.24	.130
"	1430	20.	6.6	2.3	6.2	0.90	0.76	-1.13	.140
"	1440	20.	7.0	2.3	13.0	1.7	1.1	-1.08	.150
"	1450	20.	6.1	2.4	13.8	1.1	0.96	-0.87	.190
"	1500	18.	7.0	2.1	10.0	0.99	0.80	-0.82	.160
"	1510	19.	6.1	2.1	8.0	0.95	0.78	-0.82	.140
"	1520	17.	5.5	1.7	6.2	0.90	0.75	-0.71	.110
"	1540	19.	4.8	---	4.8	0.85	0.42	-0.77	.110
"	1600	20.	4.1	---	5.0	0.63	0.67	-0.66	.090
"	1620	19.	3.7	---	---	---	---	-0.71	.055
"	1640	17.	4.0	1.4	5.2	0.72	0.64	-0.55	.083
"	1700	13.	2.2	1.7	4.0	0.62	0.66	-0.45	.098
"	1720	11.	1.7	2.2	6.5	0.90	0.57	-0.29	.160
"	1740	8.5	1.8	2.3	4.3	0.72	0.81	-0.44	.130
"	1800	8.1	1.3	3.1	3.7	0.39	0.15	-0.24	.070
2/17/77	1420	3.2	3.7	1.8	2.0	0.45	0.58	-0.24	.099
"	1440	3.5	3.7	1.1	1.8	0.30	0.20	-0.29	.091
"	1500	3.8	4.1	---	1.7	0.31	0.10	-0.19	.098
"	1520	---	4.8	2.3	1.2	0.04	0.17	-0.23	.090
"	1540	---	4.1	2.8	1.7	0.064	0.35	+0.56	.090
"	1600	---	4.1	2.0	4.0	0.40	0.46	+0.50	.087
"	1620	---	---	---	---	---	---	-----	-----
"	1720	5.2	1.5	0.77	2.3	0.28	0.032	+0.50	.098
"	1740	4.4	1.4	1.1	2.5	0.15	0.014	+1.08	.094
"	1800	5.2	1.6	1.0	2.6	0.28	0.014	+1.24	.098
"	1820	3.5	1.8	1.0	2.6	0.28	0.027	+1.40	.088
"	1840	4.0	1.9	1.1	2.8	0.30	0.010	+1.34	.095
"	1900	5.0	1.9	1.1	4.6	0.43	-----	-1.14	.110

TABLE IV

DAY	TIME	Ri ₁₀	T ₁₀ °C	U ₁₀ m/sec	q _*
2/15/77	1540	+ .10	15.25	5.33	---
"	1600	----	-----	-----	---
"	1620	+ .12	15.52	4.99	.38
"	1640	+ .21	15.49	4.51	.39
"	1700	+ .39	15.32	4.02	.34
"	1720	+ .42	15.00	3.96	.27
"	1740	----	-----	-----	---
2/16/77	1350	- .51	12.49	3.89	---
"	1400	- .39	12.43	4.07	---
"	1410	- .29	12.11	4.37	---
"	1420	- .30	11.92	4.39	---
"	1430	- .24	11.86	4.37	---
"	1440	- .20	11.98	4.93	.04
"	1450	- .10	11.88	5.84	.04
"	1500	- .13	11.84	5.24	.02
"	1510	- .17	11.78	4.90	.02
"	1520	- .24	11.81	4.18	.05
"	1540	- .26	11.76	3.86	.04
"	1600	- .34	11.96	3.45	.04
"	1620	- .97	11.71	3.00	.06
"	1640	- .32	11.89	3.17	.05
"	1700	- .19	12.10	3.56	---
"	1720	- .05	12.29	4.02	---
"	1740	- .11	12.30	4.22	---
"	1800	- .20	12.50	2.79	---
2/17/77	1420	- .10	14.69	2.93	---
"	1440	- .30	14.66	2.72	.16
"	1500	- .05	14.83	2.46	.30
"	1520	- .16	14.99	2.40	.40
"	1540	- .06	15.37	2.62	.36
"	1600	- .40	15.19	2.61	.38
"	1620	----	-----	-----	---
"	1720	+ .07	14.68	2.46	.18
"	1740	+ .33	14.30	2.40	.20
"	1800	+ .36	14.03	2.46	.22
"	1820	+ .48	13.96	2.47	.27
"	1840	+ .40	13.85	2.48	.25
"	1900	+ .22	13.83	2.84	.26

TABLE V

DAY	TIME	ΔT	X_{10}	Profile		Level 1		Z=1.0m.	
				$\partial\theta/\partial Z_{10}$	U_*	Ri	U_*	Γ	G
				10^{-2}					10^{-2}
2/15/77	1540	-.80	-.28	+ .87	.19	+ .010	.17	8.60	10.0
"	1600	----	----	----	---	-----	.15	----	----
"	1620	-1.37	-.55	+1.67	.18	+ .012	.17	2.30	3.50
"	1640	-1.65	-.81	+2.06	.16	+ .021	.13	1.60	2.60
"	1700	-1.36	-.84	+2.45	.14	+ .039	.12	1.00	3.20
"	1720	-0.97	-.62	+2.65	.13	+ .042	.12	0.82	4.30
2/16/77	1350	+0.89	+ .60	-1.50	.11	- .051	.13	2.00	5.80
"	1400	+0.85	+ .51	-1.30	.12	- .037	.13	2.70	6.30
"	1410	+1.14	+ .60	-1.19	.13	- .029	.13	2.90	3.20
"	1420	+1.31	+ .68	-1.24	.13	- .030	.13	2.70	2.40
"	1430	+1.33	+ .70	-1.13	.14	- .024	.13	3.30	2.40
"	1440	+1.18	+ .49	-1.08	.15	- .023	.17	3.60	3.00
"	1450	+1.25	+ .37	-0.87	.19	- .010	.17	5.50	2.70
"	1500	+1.27	+ .46	-0.82	.16	- .013	.15	5.00	2.10
"	1510	+1.30	+ .54	-0.82	.14	- .017	.14	5.60	2.20
"	1520	+1.26	+ .72	-0.71	.11	- .024	.13	6.00	1.90
"	1540	+1.27	+ .85	-0.77	.11	- .026	.12	6.30	2.30
"	1600	+1.31	+1.10	-0.66	.09	- .034	.12	9.60	2.40
"	1620	+1.13	+1.26	-0.71	.055	- .097	---	7.50	2.90
"	1640	+1.06	+1.06	-0.55	.083	- .032	.12	10.0	2.70
"	1700	+0.84	+0.66	-0.45	.098	- .019	.11	8.70	2.50
"	1720	+0.69	+0.43	-0.29	.16	- .005	.13	15.0	2.60
"	1740	+0.68	+0.38	-0.44	.13	- .011	.11	3.90	1.60
"	1800	+0.39	+0.50	+0.24	.070	- .020	.11	12.0	4.50
2/17/77	1420	-1.44	-1.68	-0.24	.099	- .010	.089	1.10	----
"	1440	-1.38	-1.86	-0.29	.091	- .030	.086	----	----
"	1500	-1.38	-2.28	+0.19	.093	- .005	.084	----	----
"	1520	-1.54	-2.67	+0.23	.090	- .016	.075	----	----
"	1540	-1.86	-2.71	+0.56	.090	- .006	.084	----	----
"	1600	-1.37	-2.01	+0.50	.087	- .040	.11	----	----
"	1620	-----	-----	-----	-----	-----	---	----	----
"	1720	-1.42	-2.35	+0.50	.098	+ .007	.093	1.10	1.40
"	1740	-1.00	-1.74	+1.08	.094	+ .033	.096	0.17	0.20
"	1800	-0.84	-1.06	+1.24	.098	+ .036	.097	0.18	0.69
"	1820	-0.54	-0.91	+1.40	.083	+ .048	.097	0.065	0.44
"	1840	-0.45	-0.73	+1.34	.095	+ .040	.099	0.092	0.82
"	1900	-0.17	-0.21	+1.14	.11	+ .072	.12	0.072	3.20

where

$$G = C_T^2 Z^{4/3} / \Delta T^2$$

$$\Gamma = C_T^2 / Z^{4/3} (\partial\theta/\partial Z)^2 = \text{DTSFP}$$

$$\Delta T = T_S - T_{10}$$

$$X_{10} = Z \Delta T / U_{10}^2$$

LIST OF REFERENCES

1. Businger, J. A., Wyngaard, J. C., Izumi, Y., Bradley, E. F., 1971: "Flux Profile Relationship in the Atmospheric Surface Layer," J. Atmos. Sci., 28, 181-188.
2. Cardone, V. J., 1969: "Specification of the Wind Distribution in the Marine Boundary Layer for Wave Forecasting," New York University, School of Engineering and Science, Scientific Report GSL-TR69-1, University Heights, New York, 131 pp.
3. Davidson, K. L., 1974: "Observational Results on the Influence of Stability and Wind-Wave Coupling on Momentum Transfer and Turbulent Fluctuations over Ocean Waves," Boundary-Layer Meteorology, vol. 6, 305-331.
4. Davidson, K. L., Houlihan, T., Schacher, G., and Fairall, C., 1977: "An Examination of Scaling Laws for C_T^2 in the Layer Adjacent to Ocean Waves," Proceedings, Topical Meeting on Optical Propagation Through Turbulence, Rain and Fog, Boulder, Colorado, 5 pp.
5. Davidson, K. L., Houlihan, T., Fairall, C., and Schacher, G., 1977: "Laser Propagation in the Marine Boundary Layer," NPGS Technical Report.
6. Dyer, A. J. and Hicks, B. B., 1970: "Flux Gradient Relationships in the Constant Flux Layer," Q. J. Roy. Meteor. Soc., 96, 715-721.
7. Friehe, C. A., 1976: "Estimation of the Refractive-Index Temperature Structure Parameter over the Ocean," Applied Optics, 16, 334-340.
8. Garratt, J. R., 1972: "Studies of Turbulence in the Surface Layer over Water (Lough Neagh) Part II. Production and Dissipation of Velocity Fluctuation," Q. J. Roy. Meteor. Soc., 94, 642-657.
9. Houlihan, T., Schacher, G., Fairall, C., Davidson, K., 1977: "Observational Results on Marine Fog Related Variation of Small Scale Turbulence Parameters (C_T^2 and ϵ)," Proceedings, Topical Meeting on Optical Propagation Through Turbulence, Rain and Fog, Boulder, Colorado, 5 pp.

10. Hughes, M. M., 1976: "An Investigation of Optically Revelant Turbulence Parameters in the Marine Boundary Layer," M. S. Thesis, Naval Postgraduate School, Monterey, California, March 1976, 63 pp.
11. Karch, G. W., 1976: "An Examination of Turbulent Dissipation in the Marine Boundary Layer," M. S. Thesis, Naval Postgraduate School, Monterey, California, December 1976, 72 pp.
12. Kolmogorov, A. N., 1941: "The Local Structure of Turbulence in Incompressible Viscous Fluid for very Large Reynolds Numbers," Doklady ANSSSR, 30, p. 301.
13. Lawrence, R. S., Ochs, G. R., and Clifford, S. F., 1970: "Measurements of Atmospheric Turbulence Relevant to Optical Propagation," J. Opt. Soc. Amer., 60, 826-830.
14. Marcias, V., Jr., 1977: "An Investigation of Electro-Optical Turbulence Parameters," M. S. Thesis, Naval Postgraduate School, Monterey, California, June 1977, 68 pp.
15. Monin, A. S., and Obukhov, A. M., 1959: "Basic Laws of Turbulent Mixing in the Ground Layer of the Atmosphere," Akademiia NAVK USSR, Leningrad, Geofizicheskii Institut, Trudy No. 24(151), 163-187, English Translation by Miller, J.
16. Wesley, M. L., 1976: "A Comparison of Two Optical Methods for Measuring Line Averages of Thermal Exchange above Warm Water Surfaces," J. Appl. Meteor., 15, (11), November 1976.
17. Wyngaard, J. C., and Izumi, Y., 1971: "Behavior of the Refractive-Index Structure Parameter near the Ground," J. Opt. Soc. Amer., 61, 1646-1650.
18. Volkov, Y. A., 1969: "The Spectra of Velocity and Temperature Fluctuations in the Airflow above the Agitated Sea Surface," IVZ., Atmos. and Oceanic Phys., 5(12), 723-730, Translation by J. Findley.

INITIAL DISTRIBUTION LIST

	No. Copies
1. Defense Documentation Center Cameron Station Alexandria, Virginia 22314	2
2. Library, Code 0142 Naval Postgraduate School Monterey, California 93940	2
3. Department of Meteorology Library Naval Postgraduate School Monterey, California 93940	1
4. Prof. Kenneth L. Davidson, Code 63Ds Department of Meteorology Naval Postgraduate School Monterey, California 93940	9
5. Prof. Thomas M. Houlihan, Code 69Hm Department of Mechanical Engineering Naval Postgraduate School Monterey, California 93940	2
6. Lieutenant M. M. Hughes PMS 405 Naval Sea Systems Command Washington, D. C. 20632	3
7. Lieutenant James H. Corbin Fleet Weather Central COMNAVMARIANAS Box 17 FPO San Francisco 96630	1
8. J. G. McDonald 1516 Fontana Drive Creve Coeur, Missouri 63141	1
9. Lieutenant George H. Berry Oceanographic Unit 5 USNS Harkness (AGS 32) FPO New York 09501	1

30 OCT 78
14 NOV 78

S10712
RENEWED

Thesis
C754614 Corbin
c.1

172636

Measurement of near
sea surface turbulence
and possible wave in-
fluence.

30 OCT 78
14 NOV 78

S10712
RENEWED

Thesis
C754614 Corbin
c.1

172636

Measurement of near
sea surface turbulence
and possible wave in-
fluence.

thesC754614

Measurement of near sea surface turbulen



3 2768 002 09153 0

DUDLEY KNOX LIBRARY